REPORT ON MONITORING AND SUPPORT INSTRUMENTS FOR SOLAR PHYSICS RESEARCH FROM SPACELAB

APRIL 1978

This study was performed under the auspices at the Solar Physics Quick Reaction and Special Purposes Facility Definition Team (Contract NAS 5-22368) for the Shuttle/Spacelab Payloads Project, Goddard Space Flight Center, NASA.

GODDARD SPACE FLIGHT CENTER
GREENBELT, MARYLAND

REPORT ON
MONITORING AND SUPPORT INSTRUMENTS
FOR
SOLAR PHYSICS RESEARCH
FROM SPACELAB

This study was performed under the auspices at the Solar Physics Quick Reaction and Special Purposes Facility Definition Team (Contract NAS 5-22368) for the Shuttle/Spacelab Payloads Project, Goddard Space Flight Center, NASA.

April 1978

GODDARD SPACE FLIGHT CENTER
Greenbelt, Maryland

Members of the Quick Reaction and Special Purpose (QRSP) Facility Definition Team:

L. W. Acton	Lockheed Palo Alto Research Laboratory (Chairman)
J. M. Beckers	Sacramento Peak Observatory
R. L. Blake	Los Alamos Scientific Laboratory
E. L. Chupp	University of New Hampshire
R. M. MacQueen	High Altitude Observatory
R. S. White	University of California at Riverside
C. J. Wolfson	Lockheed Palo Alto Research Laboratory

Consultants to the QRSP team:

J. -D. F. Bartoe	U.S. Naval Research Laboratory
H. S. Hudson	University of California at San Diego

The QRSP team acknowledges the assistance of the following individuals in preparing this report:

J. A. Coffman	Lockheed Palo Alto Research Laboratory
J. E. Evans	Lockheed Palo Alto Research Laboratory
R. L. Moore	Big Bear Solar Observatory
J. Roach	Ball Brothers Research Corporation
A. M. Title	Lockheed Palo Alto Research Laboratory
R. C. Willson	Jet Propulsion Laboratory

CONTENTS

CONTENTS (continued)

ILLUSTRATIONS

ILLUSTRATIONS (continued)

TABLES

REPORT ON
MONITORING AND SUPPORT INSTRUMENTS
FOR
SOLAR PHYSICS RESEARCH
FROM SPACELAB

1.0 INTRODUCTION

The advent of orbiting instrument carriers has made the entire electromagnetic spectrum available to the astronomer and permits avoidance of the inevitable image degradation produced by the Earth's atmosphere. In the near future, the payload capacity of Spacelab will allow the use of large and powerful sets of telescopes to take full scientific advantage of this fact.

In the discipline of solar physics, almost all observational investigations will require the availability of certain ancillary and correlative information such as:

- Full-disk images of the photosphere, chromosphere, transition region, and corona for the purpose of target selection, monitoring of solar activity, and atmospheric structure
- Photospheric magnetograms with good sensitivity and spatial resolution
- Chromospheric filtergrams and velocitygrams with good spatial and time resolution for recording the detailed dynamical and structural context of the primary observations
- Full-disk spectral irradiance measurements to quantitatively establish the output and time variability of the solar radiation

This report describes a minimum set of three solar research support instruments for Spacelab that are intended to provide the above sorts of information. As noted, such data are important to most solar and solar-terrestrial investigations but are not normally provided by the primary telescopes.

The Quick Reaction and Special Purpose Facility Definition Team (QRSP-FDT) for Solar Physics Spacelab Payloads has examined a variety of instruments to fulfill the following functions: solar physics research appropriate to Spacelab, correlative data for research in such fields as aeronomy, magnetospheric physics, ionospheric physics, meteorology and climatology, target selection for activity alert monitoring and pointing accuracy monitoring of Spacelab platforms. In this examination the team has accepted a number of restrictions and qualifications: (a) the cost of such instruments must be low, so as not to adversely impact the development of new, research class instrumentation in the early Spacelab era; (b) the instruments should be of such a size that they each would occupy a small fraction ($\sim 1/8$) of a pointing system (SIPS); and (c) the weight and power consumption of the

instruments should also be small. With these restrictions, the instruments chosen are: the visible light telescope and magnetograph, the extreme-ultraviolet (XUV) telescope, and the solar irradiance monitor.

The visible light telescope, equipped with narrow-bandpass, tunable-birefringent filters (one of which covers the Hα line and both the wings) is a very versatile instrument that can be used to study the short-term morphology and evolution of magnetic, velocity, and intensity features of the quiet Sun, growing and decaying active regions, and of coronal hole areas. The wavelength resolution will be high enough to reconstruct line profiles.

The XUV monitor provides television (TV) or photographic images of a variety of high-temperature phenomena in the solar atmosphere. The ability to view features in the chromosphere, transition-region, and corona is important in several areas of solar physics research where the XUB monitor's high-resolution and rapid-cinematographic sequence will provide insight into dynamic three-dimensional processes. This instrument will also serve a number of operational purposes, such as detecting preflare activity and forewarning the onset of flares by several minutes.

The solar-spectral irradiance monitor will be used in studies of the solar energy budget, and the contributions and fluctuations occurring in different wavelength regions and in different spectral features. The fluctuations of certain spectral features will provide insights into solar dynamic processes. The careful monitoring of these emissions and their fluctuations will provide a solar activity alert, and support measurements for aeronomy, ionospheric physics, meteorology, and climatology experiments and studies.

Each of these instruments will be discussed in the following sections of this report in terms of scientific objectives, and typical geometrical, operational, and performance. The QRSP Team has *not* considered the relative merits of all possible types of instruments available in each of the categories and this document should not be construed as a judgment in that regard. Rather, extensive discussion within the team has resulted in the selection of this minimum compromise set of representative instruments which have then been studied for performance and feasibility in greater detail.

This report resulted from initial efforts by the QRSP-FDT to define a "Solar Monitor Package" for Spacelab. To prevent confusion it is worthwhile to emphasize that these instruments do not, in fact, constitute a solar monitor package in the sense of our original concept, although they may individually or collectively perform monitoring functions as required for a given Spacelab mission. Also, the term "package" is a misnomer because the three instruments are functionally independent and the choice of which one(s) to utilize would be mission dependent. This report reflects the unanimous conclusion of the Team that a limited selection of relatively sophistricated general-use support instruments, rather than a monitor package *per se*, is what will be most needed to support solar physics and solar-terrestrial research from Spacelab.

SECTION 2

VISIBLE LIGHT TELESCOPE

AND

MAGNETOGRAPH

ACKNOWLEDGMENTS

J. M. Beckers of Sacramento Peak Observatory developed the original conceptual design for a Spacelab Visible Light Telescope and Magnetograph. This design was further developed and refined by A. M. Title, H. Ramsey, and R. Smithson of the Lockheed Solar Observatory to the form presented here. L. W. Acton and J. E. Evans of Lockheed assisted in the preparation of this report.

2.0 VISIBLE LIGHT TELESCOPE AND MAGNETOGRAPH

2.1 INTRODUCTION

This report on the Visible Light Telescope and Magnetograph discusses the scientific importance of the measurements to be made with this instrument and the geometry, performance, and operation of the instrument. This telescope will play a role both for primary solar physics research and in obtaining correlative data for other experiments in solar physics and allied fields. It will also monitor pointing accuracy of Spacelab instrument platforms to subarc-sec accuracy.

The scientific objective is to obtain information on the spatial scale and temporal evolution of solar magnetic and velocity fields, to learn about the mechanisms by which magnetic flux emerges through the solar surface, is distributed, and decays, and to acquire data on transient events such as flares. This will be done with a narrow bandpass, tunable, birefringent filter capable of operating in spectral lines having differing magnetic and temperature sensitivities. The filter bandpass will be sufficiently narrow (60 mA FWHM) to permit reconstruction of line profiles.

With filtergrams obtained from the quiet Sun, growing and decaying active regions, and from coronal hole areas, it should be possible to study the short-term morphology and evolution of magnetic, velocity, and intensity features in each of these areas. Spacelab based measurements can avoid image degradation produced by the Earth's atmosphere and interruptions caused by poor seeing, weather, and even by nightfall when a constant Sun orbit is used.

2.2 EXPERIMENT OBJECTIVES

The solar magnetic and velocity field measurements program planned for Spacelab has the following typical scientific objectives:

- To measure magnetic and velocity fields in the solar atmosphere with spatial resolution greater than can be achieved from the ground and to deduce from these observations the small-scale structure and evolution of individual magnetic elements on the 10 to 20 min time scale of solar granulation
- To follow the evolution of solar magnetic structures over periods at least comparable to the 20- to 40-hr lifetime of supergranules to determine how the magnetic elements couple to the supergranule velocity patterns and by what mechanisms field diffusion and disappearance occur
- To study with high-temporal and spatial resolution the magnetic field changes associated with transient events, such as flares, and to isolate and follow the birth of sunspots, pores, and ephemeral regions

Magnetic fields play a crucial role in determining the structure and dynamics of the solar atmosphere, from the deepest visible levels of the photosphere, upward through the chromosphere and corona, and out into the interplanetary medium. Magnetographs and velocitygrams of smaller features of the solar surface taken from the Earth's surface have proven very difficult to interpret, primarily because of blurring and distortion of images by the Earth's atmosphere. Conflicting results are often obtained when different aperture sizes, spectral lines, or calibration procedures are used. Most magnetographs measure mean flux in resolution elements 700 to 4000 km (1 to 6 sec) across, and thus average over a rather large area on the solar surface. Since the weighting of these averages is unknown, only crude limits can be set on important physical properties such as temperature, velocity, magnetic field vector, and energy density.

Despite the presence of several superb ground-based facilities, little further advance can be expected in defining the details of the small-scale structures due to the inherent limits imposed by atmospheric seeing. A major advantage of space is the absence of atmospheric inhomogeneities. In ground-based observations, seeing has two important effects: one is blurring, and the other is image distortion. The former limits spatial resolution, while the latter prevents the superposition and direct comparison of sequential images. Even during the times of best seeing, local image distortions of 1 to 2 sec mask any real changes which may be present on the subarc-sec scale. A pair of filtergrams taken from the ground with recently developed techniques is shown in Figure 2-1.

Observations on small-scale fields have shown that the network is composed of small, unresolved magnetic points. The magnetograms seen in Figures 2-2 and 2-3 are derived from the filtergrams in Figure 2-1, and indicate that the magnetic points are organized into a small-scale network with cell sizes of 2 to 3 sec, and that these cells, in turn, form the larger network cells. Even in these exceptional pictures, probably the highest resolution magnetograms ever obtained on the ground, the magnetic points are barely discernable because of atmospheric seeing. (It is worth noting that these filtergrams were made recently using a filter which a study by the QRSP Team has shown to be readily space hardenable.) With high-resolution lines profiles, accurate field strengths, and measures of the fraction of the resolved area covered by the field can be obtained along with information on the field vector, the temperature, and the velocity structure. Energy densities and stresses can be inferred from these measurements to evaluate theories of confinement. Most theorists find it difficult to understand the existence of kilogauss fields in subarc-sec flux tubes.

Magnetic and velocity oscillations with periods of a few minutes are observed in sunspots, and their energy transport is crucial for spot formation, according to current theories. Do similar waves occur in the network fields that contain overall much more flux than the spots? If so, what role do they play in coronal heating or pore formation? Although the resonant 5-min oscillation has been detected in ground-based magnetograms, very little is known about its spatial structure or efficiency in transporting energy. Again, the necessary observations can only be obtained with a space telescope.

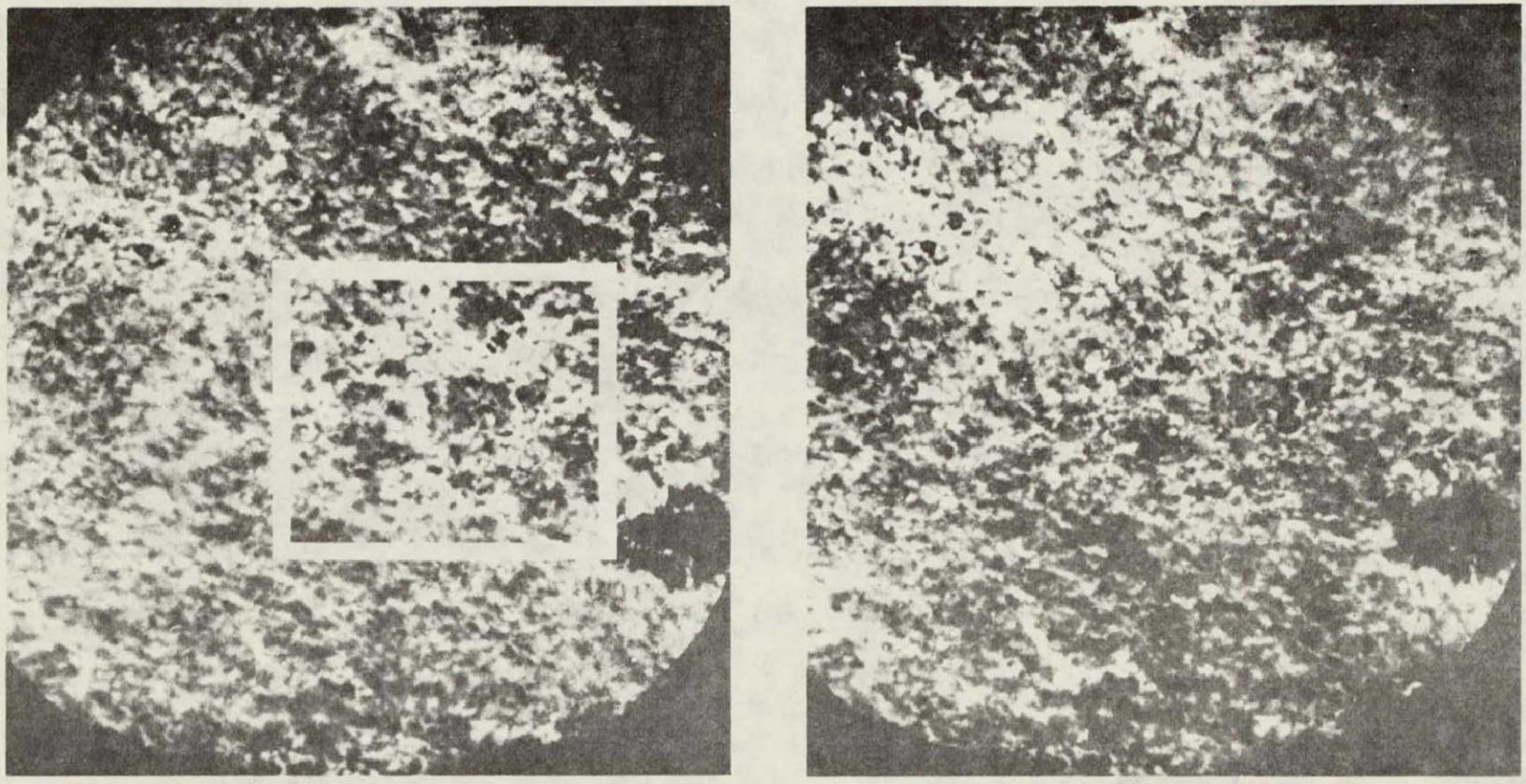

Figure 2-1. A Pair of Filtergrams Taken with the Lockheed Tunable Filter at Sacramento Peak with 30" Vacuum Tower Telescope (Filtergrams are in right and left circularly polarized light at 0.04 Å to the blue side of Fe I 6302. The circular edge is a field stop—not the solar limb. The diameter of the field is 138 arc-sec. The white box outlines the area whose magnetogram is shown in Figure 2-2.)

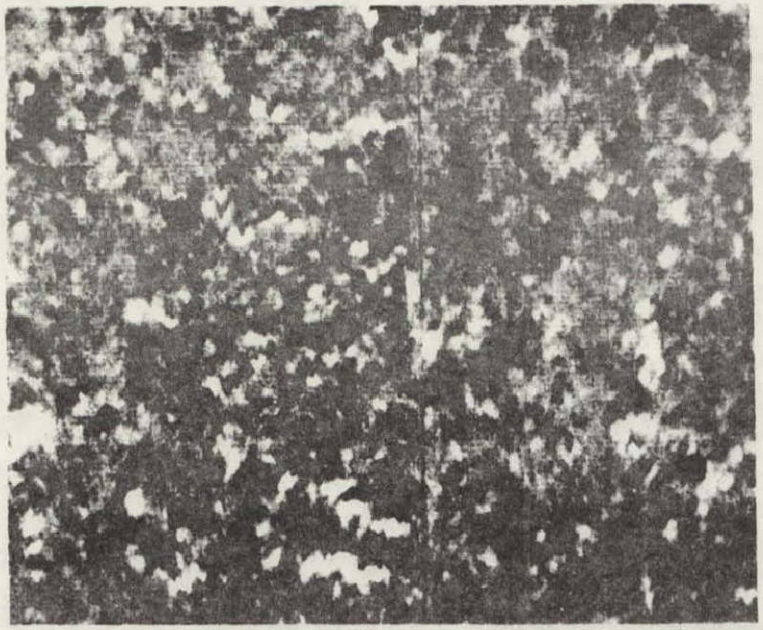

Figure 2-2. Photodigital Magnetogram from Filtergrams Shown in Figure 2-1 (Magnetogram is made by microdensitometering the filtergrams, digitally subtracting the images, and scaling the data, and generating the result via the "playback" mode. The width of the magnetogram is 50 arc-sec. The tick marks are 1 in. apart.)

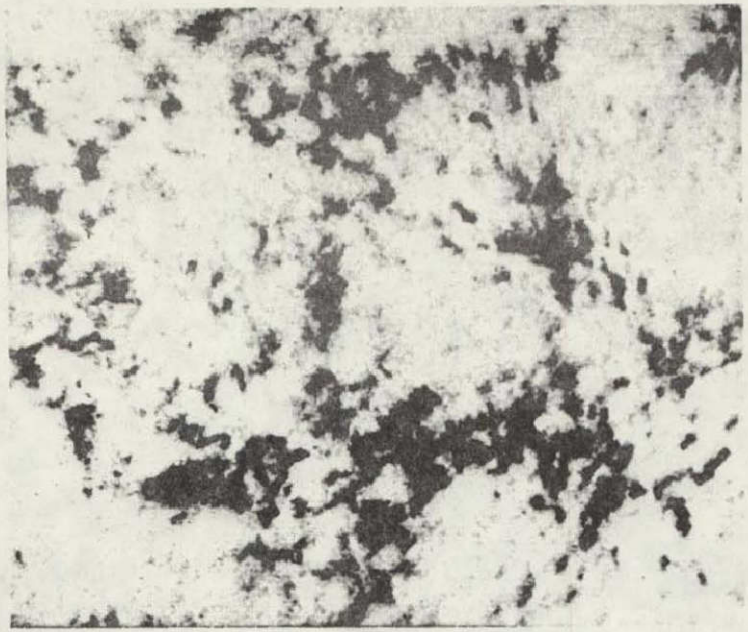

Figure 2-3. Section of Typical High Signal-to-noise Ratio Magnetograph Taken with KPNO Diode Array Magnetograph (The width of the magnetogram is 240 in.)

Magnetic field changes in the photosphere during flares have not been documented but they are expected to occur. There will be Spacelab missions near the peak of the next solar cycle when the expected effects should be strongest. The observing program should include a period of operation in flare patrol mode.

It is generally accepted that the concentrated magnetic fields in active regions are dispersed by a random-walk process caused by supergranulation. The magnetic network exists as flux concentrations at the boundaries of supergranule cells. Very few observations of motions of these network flux points exist. The basic time scale for changes in the network is 20 to 40 hr and thus the complete evolution is difficult to follow from the ground. The precise mechanism and rate of flux dispersion remain uncertain, but there is some evidence that the rates of flux diffusion and annihilation in active regions and filament channels may be different from that in the network. If we can monitor active regions, network, filament channels, and coronal holes at 1 to 3 hr intervals over a 20 to 40 hr period, there is an excellent chance that these matters can be clarified.

2.3 OPTICAL INSTRUMENTATION

The optics evaluated for the Spacelab Visible Light and Magnetograph System are shown schematically in Figure 2-4. The cassegrain reflector is used because it makes the design much more compact. A parallel optical train is used for the full-disk system because it considerably simplifies the optical system and permits continuous monitoring and recording of full-disk Hα information even when the magnetograph is being used.

The primary image detectors for the system are 512 by 512 or larger CID arrays. These devices should be available shortly; 800 by 800 devices have been developed under government contract and are currently available to NASA and DOD users. Each array system has associated with it a film camera for permanent image recording. In addition, we envision a high-precision CRT that is imaged onto another film focal plane to record magnetograph output in a permanent form.

Basically, the optical system produces a full disk 0.5 Å image (35 ft field of view) through the Fabry-Perot system. Simultaneously, a 1/6 Å birefringent system can produce images of 4 or 8 arc-min at any wavelength within the range transmitted by the 800 Å entrance blocking filter, depending on the choice of internal blocking filters. Interesting wavelengths, for example, are λ5876, 5896, 6103, 6303, and 6563 Å. The 1/6 Å images can be processed by the magnetograph electronics to form both magnetograms or velocitygrams. In addition, the full-disk Hα image can be stored so that past versus present Hα images can be blink compared on the display console, or Hα differences can be displayed using the magnetograph electronics. As suggested above, the processed images can be permanently recorded on film.

The magnetograph envisioned would be similar to the Smithson diode-array system.[1] However, this magnetograph would have the 512 by 512 element images stored rather than 512 by 1 as in the current magnetograph. In addition, there would be two additional 512 by 512 image memories. One would be normally used for the "past" Hα full-disk image and the

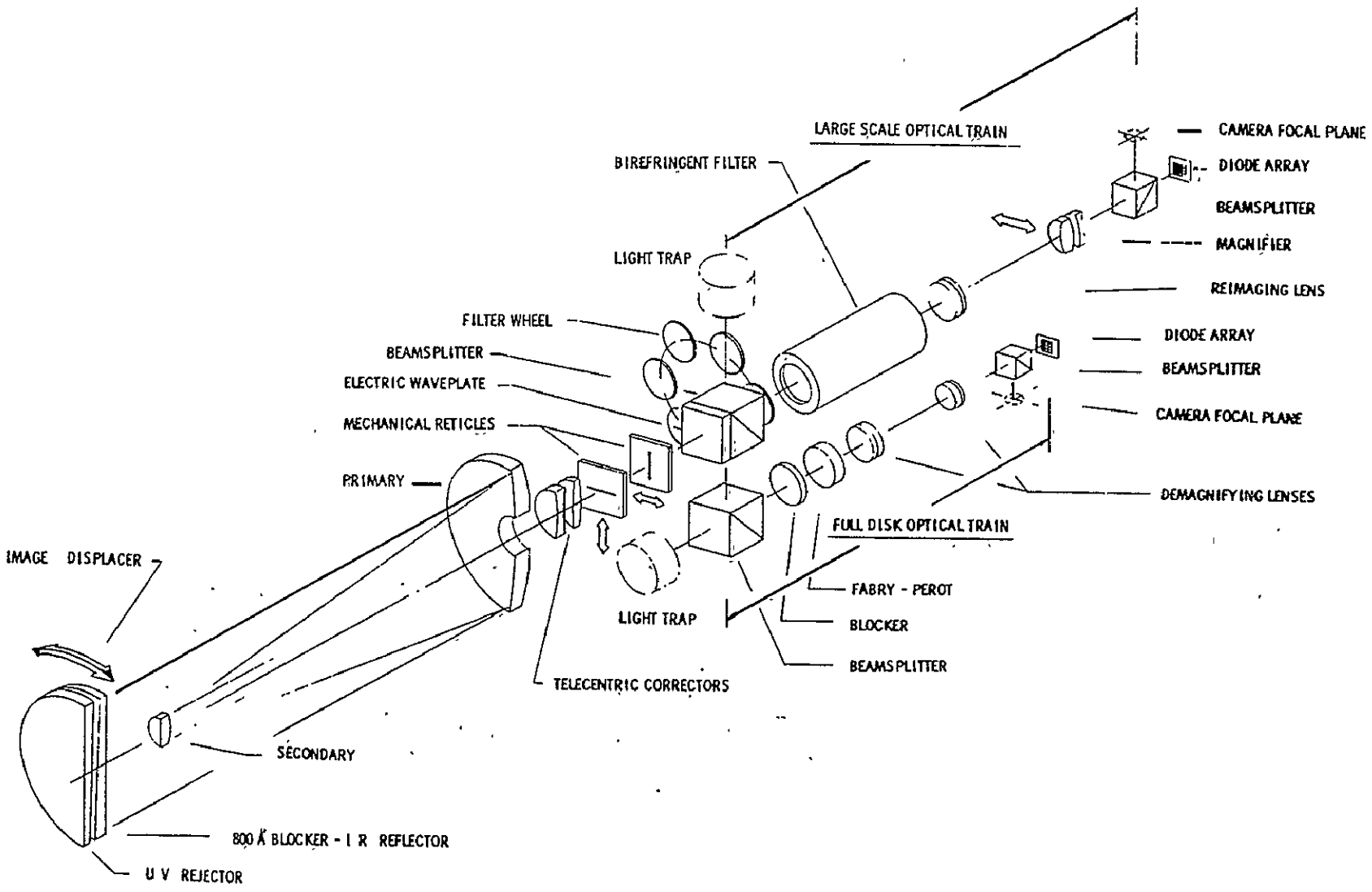

Figure 2-4. Hα/Magnetograph Optical Schematic

other for a "past" magnetogram or velocitygram. The light paths are shown in Figure 2-4, and discussed in more detail in paragraph 2.4.

2.4 DETAILS OF THE LIGHT PATH

In following the light through the telescope, the first element is a 20-cm diameter plate that has a dielectric coating on its first surface to reflect light short of 4500 Å. The purpose of the coating is to protect the Zn layers in the dielectric coating in the blockers that follow. The element is made of BK-7 and has a slight wedge so that, by rotating this element and the following element, the solar image can be displaced by a solar radius in any direction. The rear surface has an antireflection (AR) coating. The second element is identical to the first, except that it has an 800 Å bandpass filter centered at λ6200 Å. The filter is of the induced transmission type and contains a thin silver layer that serves to reject the entire infrared spectrum. Both the ultraviolet (UV) rejector and the induced transmission filters are the same as flown on the Skylab mission.

The next set of elements is the f/30 cassegrain with telecentric correctors and mechanical reticles. This unit is modeled on the cassegrain section of the Perkin-Elmer Skylab Hα system. It has a 16.5-cm aperture and produces an f/30 telecentric image. It has the additional advantage of having a mechanical reticle assembly in the focal plane. The reticle consists of a pair of BK-7 plates that can be driven in orthogonal directions. The Skylab reticle assembly has orthogonal straight lines. Immediately behind the reticle assembly is an electric waveplate and a polarizing beam splitter that serves as the entrance polarizer for the birefringent filter and part of the folding system for the full-disk Hα system.

In following the light through the birefringent system, after the beam splitter, the beam encounters the blocking filter wheel. This wheel contains six 10 Å (1.8-cm dia) blockers centered at λ5876, 5896, 6103, 6302, 6563 Å and a position for a spare filter or filter for another line. The front and rear windows of the filter wheel assembly have crossed quarter waveplates mounted on them. Straight through light is unaffected; however, reflected light passes through the first quarter waveplate twice and thus has its plane of polarization rotated by 90 deg. The reflected beam is thus deflected upwards by the beam splitter into a light trap.

The transmitted beam travels through the 1/6 Å birefringent filter (described later). Mounted at the end of the filter is a one-to-one reimaging lens that forms the final image upon the diode array or film camera focal planes. The pair of focal planes are created by a beam splitter immediately before the final focal plane. Both focal planes are 1.3-cm square and cover 8 arc-min of the solar surface. The image scale in the birefringent system can be expanded by a factor of two by mechanical insertion of a positive-negative magnifier assembly. The array then covers 4 arc-min of the solar surface. The film system can accomodate the increase in field.

The full-disk light travels downward from the first polarizing beam splitter and is folded parallel to the optical center line of the birefringent system, but 8.9 cm below it, by the second polarizing beam splitter. The light then strikes a quarter waveplate mounted on the

window of the blocker Fabry-Perot assembly. The reflected light is rotated in polarization state by 90 deg; it travels straight through the second polarizing beam splitter, and is absorbed by a light trap. The transmitted beam goes through the blocker and then through the 0.5 Å Fabry-Perot. On the back of the Fabry-Perot filter package is a 46-cm focal length lens that images the objective on a 11.5-cm focal length lens. The ratio of the focal lengths 46/11.5 = 1/4. This combination then demagnifies the primary image. The demagnified image passes through a beam splitter and onto an array and film focal plane. Both focal planes cover a 35 arc-min field of view.

2.5 BIREFRINGENT FILTER

This design is based on the Lockheed Universal Filter which was used for Figures 2-1 and 2-2. This device has 38 percent transmission in polarized light and utilizes plastic achromatic waveplates. The birefringent filter would use achromatic half-waveplates for the wide-field elements and for tuning the filter. Each element would also have a quarter waveplate on it for tuning purposes. Figure 2-5 shows an exploded view of a section of the filter. The filter has four such sections that differ only in crystal lengths.

Tuning would be accomplished by rotation of half-waveplates only. All of the calcite elements would be shock mounted in a fixed orientation. For the wavelength range of this filter, antireflection (AR) coating on all exterior surfaces should be very nearly as good as oil fill. If AR coating is used, then the filter would not be oil filled. The rotation of the elements could be accomplished with either stepping motors or with servomotors and an optical encoder. The servomotor system has the advantage of using less power and dissipating less heat. If an oil filled design is used, hermetically sealed rotary actuators are available so that rotary oil seals are not required.

A filter with a free spectral range of 10 Å and a full width of 1/6 Å seems to be a good choice. Either a contrast element Lyot design or an alternate partial-polarizer design would be adequate. The alternate partial-polarizer design has the advantage of higher transmission and better rejection than the contrast-element design. Both filters would require eight elements.

From the initial studies, it seems prudent to both thermally enclose the filter and to sense the temperature of each element. The computer would then make tuning compensations for thermal excursion or gradients.

2.6 ELECTRONICS

The telescope electronics include three major subsections: (1) telescope operations, (2) operator displays and controls, and (3) magnetograph processor. Included in telescope operations are offset pointing, camera selection, magnification selection, and filter operations. Operator controls and displays include the video monitors and the keyboard controls that command the telescope and processor. Ground control would be identical to payload specialist control. The magnetograph processor will handle all the image processing of the array outputs.

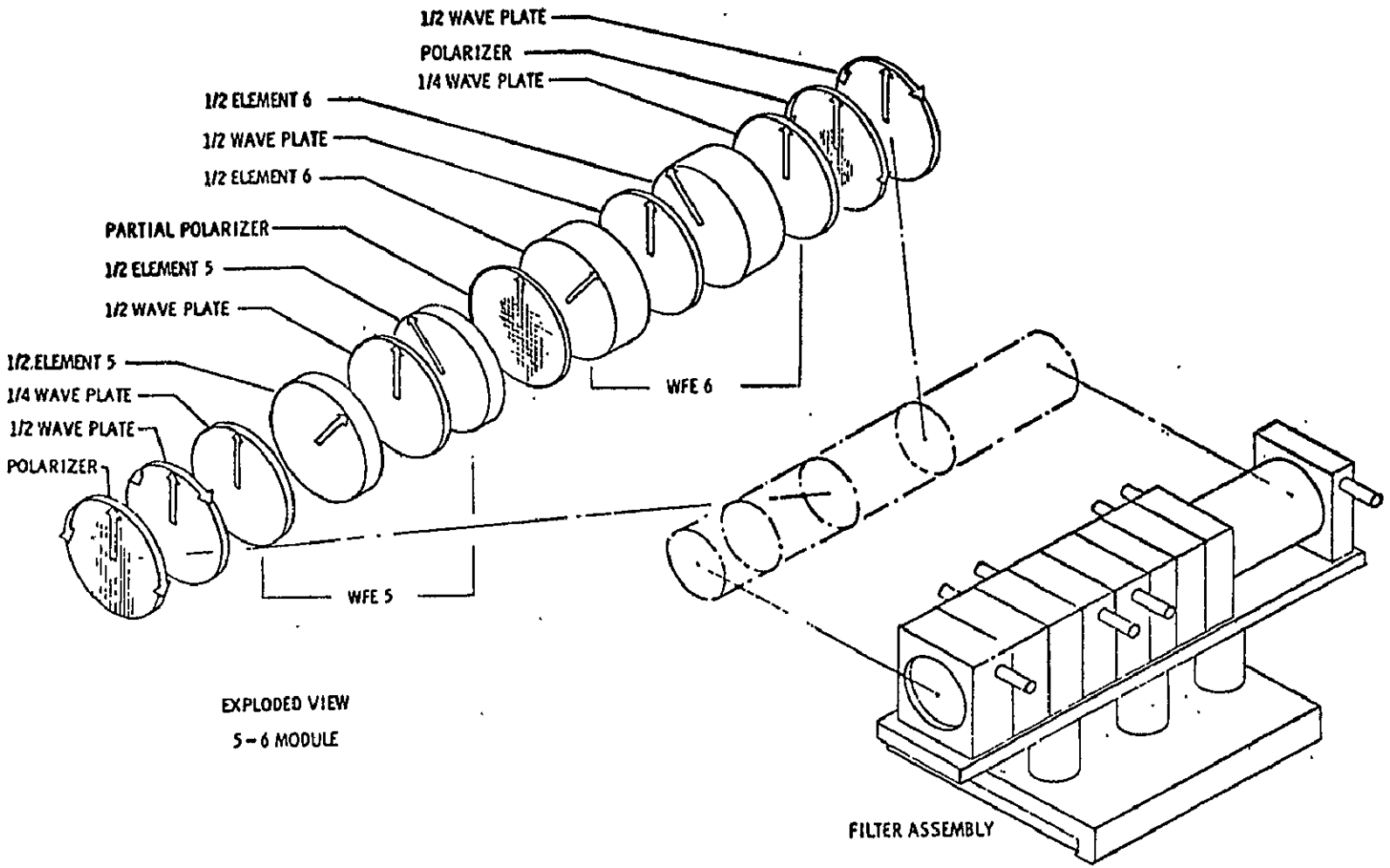

Figure 2-5. Electro-mechanical Schematic for a Computer Controlled Tunable Filter

The hardware would consist of a microprocessor, such as an LSI-11, that would communicate with the onboard operator through the keyboard or the ground through the downlink. The computer would control the telescope operations and the image processor.

The magnetograph processor would consist of a ring-memory image storage for three images and a hardwired subsystem that would allow addition, subtraction, division, and multiplication operations on the array output and the stored images.

SECTION 3

EXTREME ULTRAVIOLET MONITOR TELESCOPE

ACKNOWLEDGMENTS

This Extreme Ultraviolet (XUV) support telescope study was prepared by John-David F. Bartoe of the U.S. Naval Research Laboratory and N. Paul Patterson of Ball Brothers Research Corporation with support from G.F. Brueckner (NRL) and D. F. Schneible, M. Garin, and W. A. Delemere (BBRC).

COMMENTS

"I was very impressed with the XUV Monitor in that . . . it showed by bright areas the exact location of active regions."

Dr. Joe Kerwin, Skylab 1/2
Technical Crew Debriefing

"In my own case, and I expect Jack [Lousma] and Al [Bean] did the same, I tried to use the XUV Monitor as the decision instrument for . . . pointing instruments. . ."

Dr. Owen Garriott, Skylab 1/3
Technical Crew Debriefing

"I thought that [ATM-XUV Monitor] was exceptionally useful . . . The more I think back on that, the more I realize how valuable that display was for picking out locations at which to make observations as well as for flare detection."

Dr. Ed Gibson, Skylab 1/4
Technical Crew Debriefing

3.0 EXTREME ULTRAVIOLET MONITOR TELESCOPE

3.1 INTRODUCTION

At the request of the Solar Physics Spacelab Quick Reaction and Special Purpose Facility Definition Team (SPSQRSP FDT), the following study was performed to design an extreme ultraviolet (XUV) monitor that can produce a real-time image of the full solar disk in the 200 to 600 Å wavelength region with high spatial resolution. The particular performance requirements set forth by the SPSQRSP FDT are as follows:

- Spectral coverage—200 to 600 Å with broad band filters
- Field of view—full disk (32 arc-min)
- Spatial resolution—5 arc-sec or better
- Real-time video display (~1 min update time)
- Secondary film recording
- Low cost

No existing XUV monitor can meet all of these requirements. Consequently, a new instrument has been designed. However, existing hardware and proven design concepts have been employed throughout. The design meets the operational objectives of an XUV Monitor Support Telescope and, at the same time, meets certain scientific objectives of XUV solar research.

3.2 EXPERIMENT OBJECTIVES

XUV monitor provides TV or photographic images of a variety of high-temperature phenomena in the solar atmosphere. The ability to view features in the chromosphere, transition-region, and corona, such as those seen in Figures 3-1 through 3-4, serves a number of operational purposes, and the analysis of such data contributes to several areas of solar physics.

The principal value of a high-resolution XUV monitor is the insight into dynamic three-dimensional processes that its continuous display or rapid cinematographic sequence provides the observer. In the XUV, normal-incidence reflective optics maintain high spatial resolution over a wide field of view. Strong XUV line emission and efficient optics result in a compact instrument with high-time resolution. Filters separate chromospheric from higher temperature features. Instabilities in magnetic arches of active regions, which appear as subflare brightenings in transition-zone emission lines, can be observed. In the XUV, the relatively narrow range of coronal temperatures ($1\text{-}2 \times 10^6$ K) recorded by the instrument provides well-defined images. On the other hand, emission from the extremely hot ($15\text{-}20 \times 10^6$ K) core of a flare is also recorded.

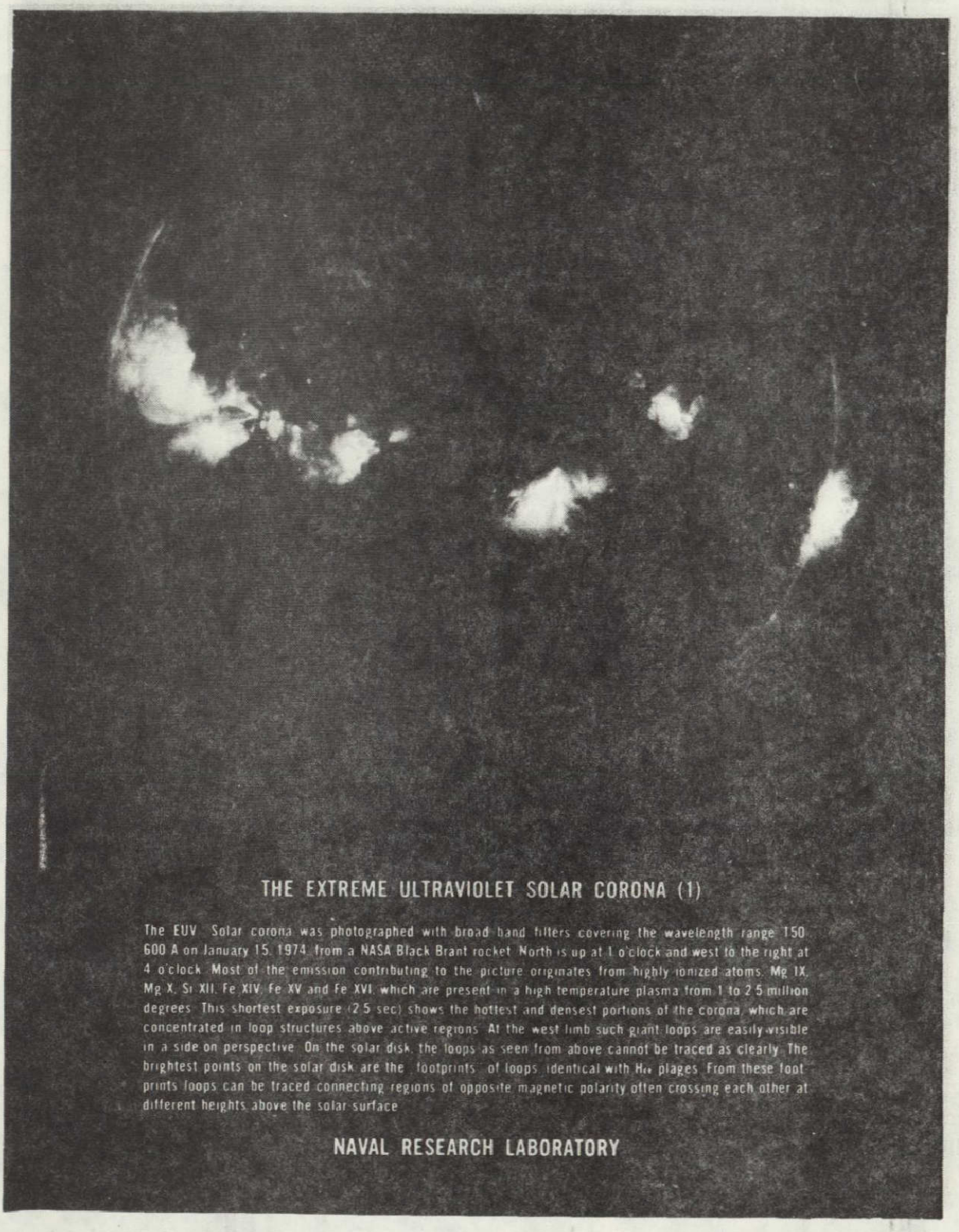

Figure 3-1. The Extreme Ultraviolet Solar Corona (1)

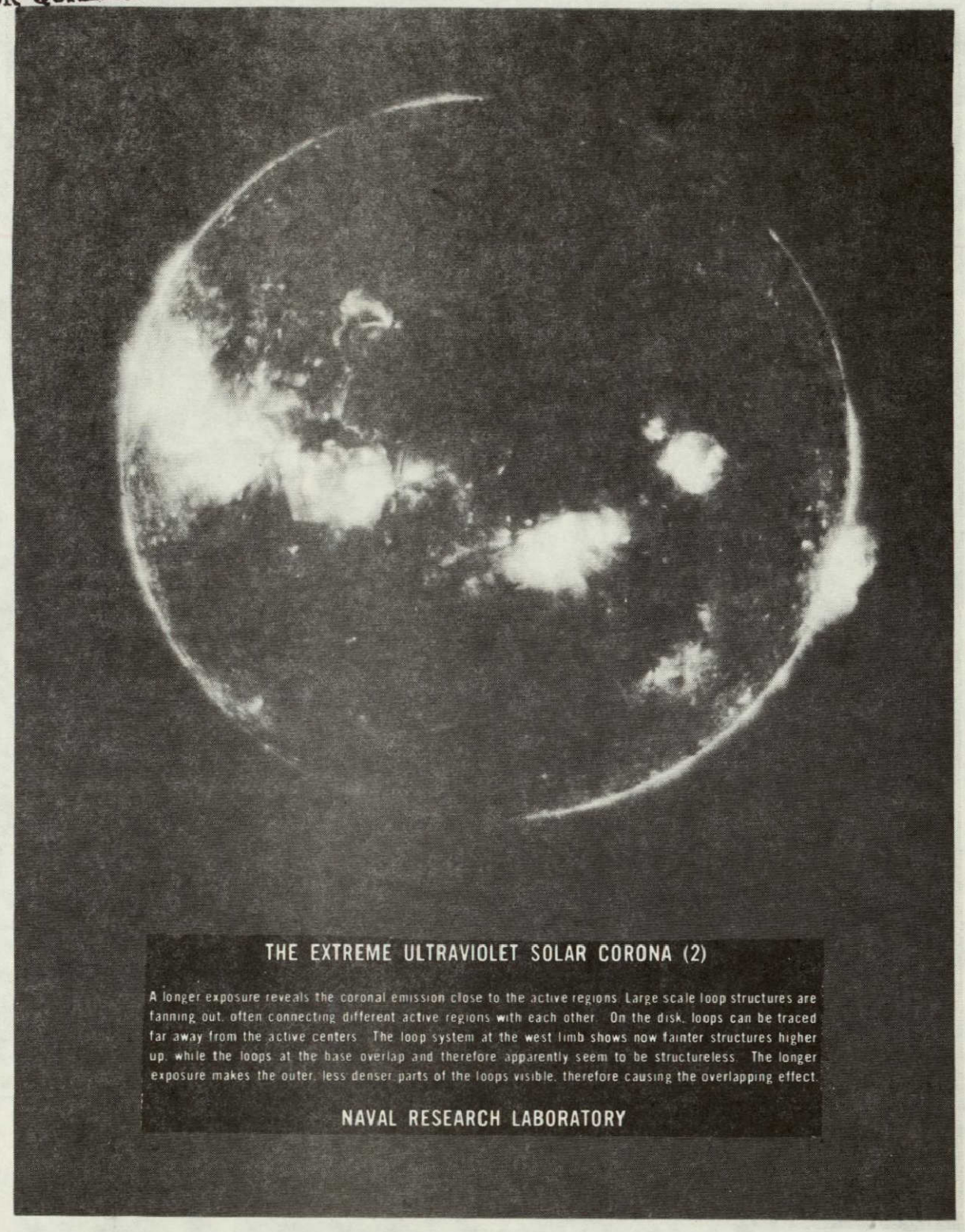

Figure 3-2. The Extreme Ultraviolet Solar Corona (2)

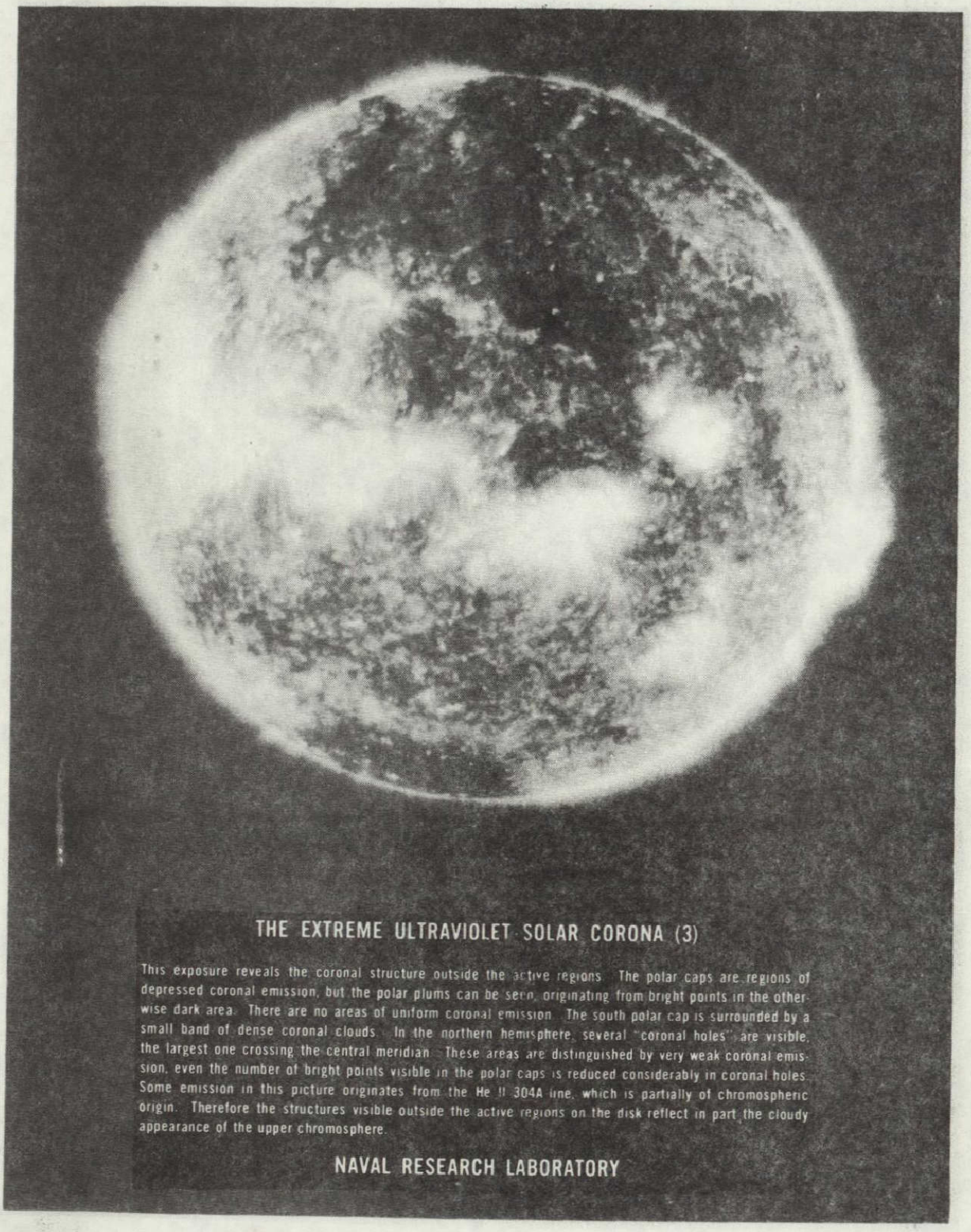

Figure 3-3. The Extreme Ultraviolet Solar Corona (3)

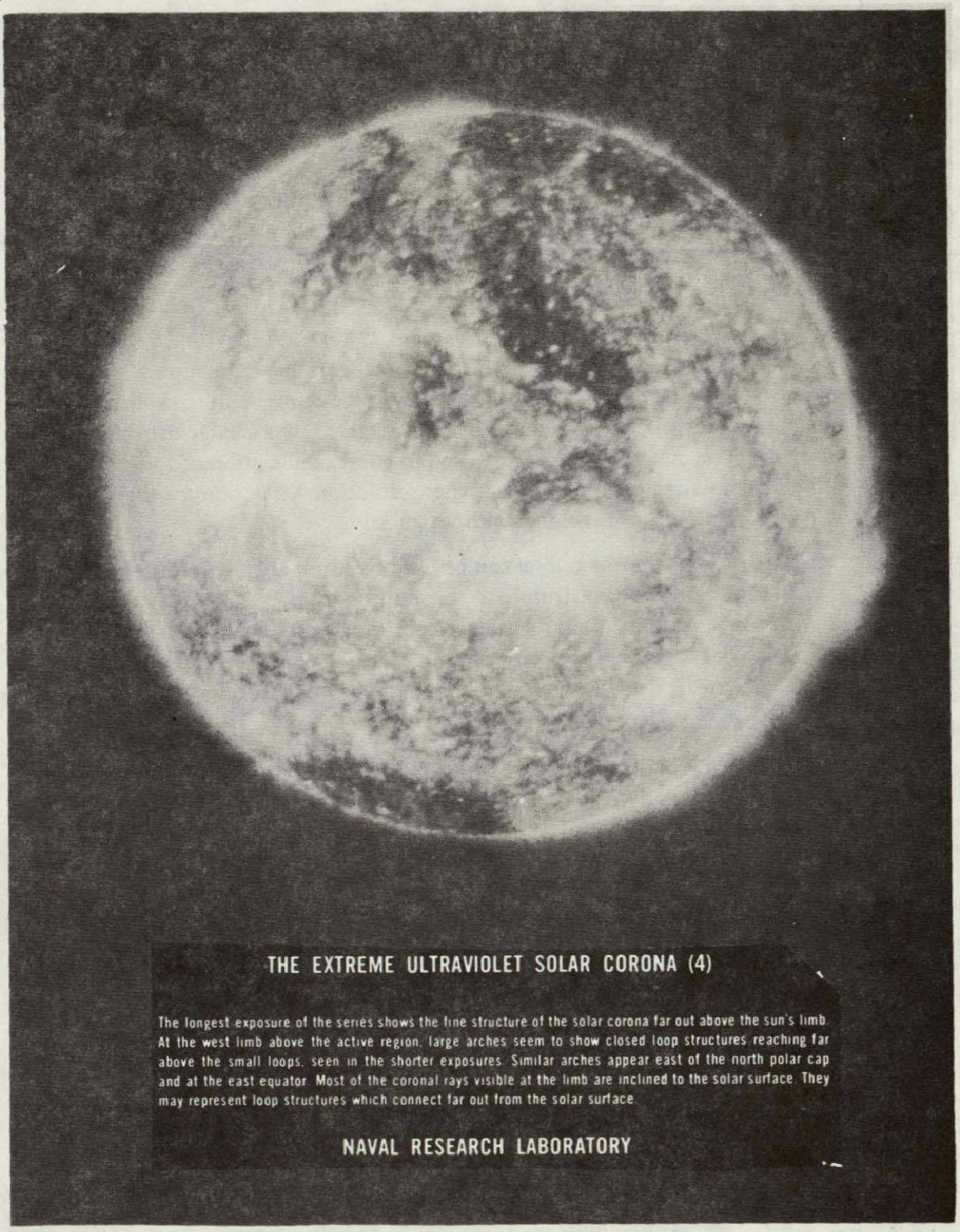

Figure 3-4. The Extreme Ultraviolet Solar Corona (4)

The clarification of several phenomena observed on Skylab will accompany improvements in spatial resolution. This section is a summary of uses to which such an instrument can be put, extrapolating from the Skylab experience.

3.3 OPERATIONAL OBJECTIVES

Whether a sun-pointed payload is being controlled from the ground or payload specialist station, a real-time XUV display will enhance the interactive capability of the operator, enabling him to visualize otherwise invisible solar features and respond to unpredictable events.

3.3.1 Flares

As a flare detector, an XUV monitor provides an instantly recognizable indication of the onset of high-temperature emission from a flare anywhere on the Sun. Figure 3-5 shows an example of the pointing for the flare of June 15, 1973, selected by a Skylab astronaut. The double ribbons visible on an Hα monitor were used to guess the location of the high-temperature volume of the flaring region. With a higher resolution XUV monitor than was available, he could have pointed to this volume without guessing.

A threshold detector that senses the video level can be used to automatically initiate pre-programmed "Flare Modes" in various instruments. In addition, the pixel address of the flaring feature can provide a digital readout of its exact position on the solar disk. This can be used for recording activity histories of specific sites in each active region, as well as for automatically slewing narrow field-of-view instruments to the proper location.

By means of an overall increase in the brightness of an active region, and quasi-periodic (30) to 90 sec) fluctuations in the brightness of tiny points on opposite sides of the neutral line, Skylab astronauts learned to anticipate the onset of flares. This preflare activity provided them with several minutes of forewarning. At higher spatial resolution, it should be possible to sharpen this subjective technique.

3.3.2 Identification and Pointing

The passband of an XUV monitor would include emission from the chromosphere, transition-region, and corona. By introducing an Al+Te filter, the contributions of He I 584 Å and He II 304 Å in the XUV image can be greatly reduced. This almost eliminates the superposition of chromospheric (2-8 X 10^4 K) features and hotter features, and allows details seen in Hα, XUV, and soft X-ray images to be correlated spatially.

The extension of Hα features, such as individual network cell boundaries and prominences, can be traced out into the corona, where the XUV monitor cross-hairs can be used for pointing. Figure 3-6 shows, in He II 304 Å, the chromospheric network, a prominence, and several loops in an active region at the limb.

Precise pointings in coronal holes, filament cavities, individual loops in and between active regions, plumes, bright points, and otherwise invisible high-temperature features can be

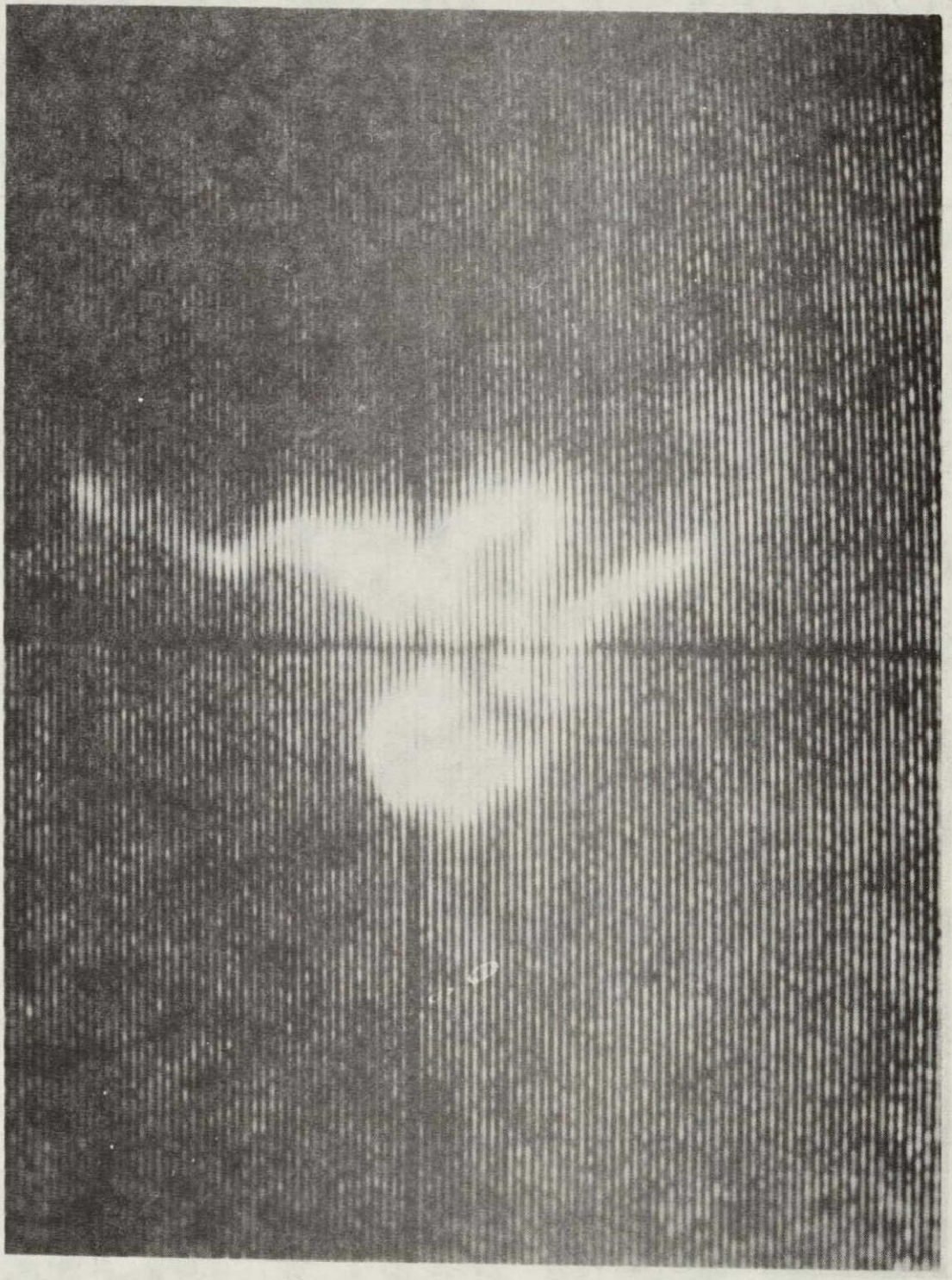

Figure 3-5. Flare of June 15, 1973

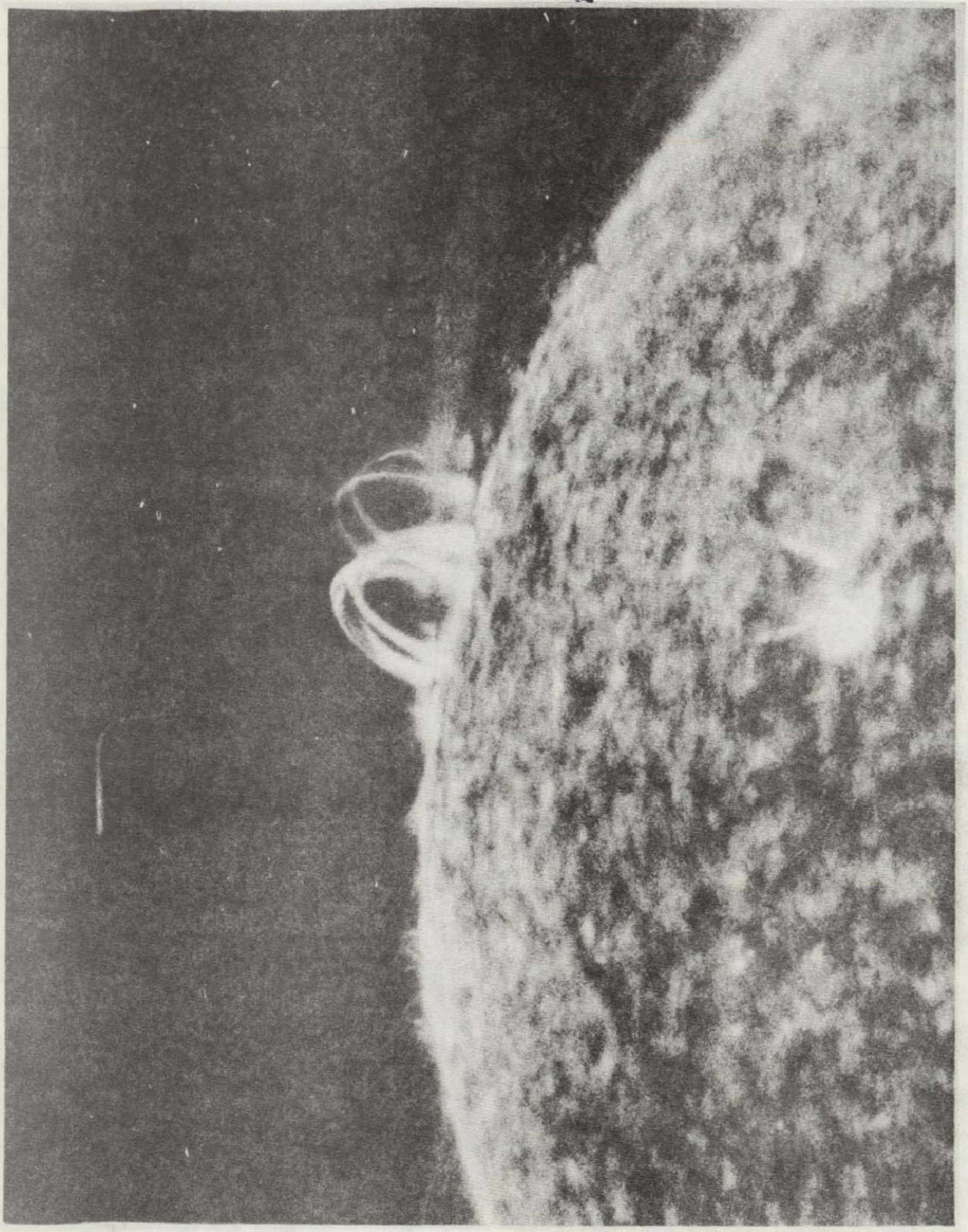

Figure 3-6. A Prominence and Several Loops in an Active Region of the Chromospheric Network

similarly carried out. With integration, helmet streamers may be traceable through the inner corona, using a narrow field-of-view mask to eliminate disklight scattering in the detector.

If particular locations in XUV images of active region loops are identified as the sources of hard X-ray bursts, hard X-ray instruments can be pointed at these locations with the crosshairs of an XUV monitor.

3.3.3 Coalignment of Visible, XUV, and X-ray Instruments

By means of XUV bright points in the chromospheric network, Hα, XUV, and soft X-ray imaging instruments can be coaligned. Using the inner edge of the shell of XUV emission around the disk, where the abrupt reduction in the line of sight decreases the intensity, the misalignment of visible, XUV, and X-ray, nonimaging instruments can be determined to within a few arc-sec, permitting offset pointing or coalignment with the crosshairs of imaging instruments.

3.4 SCIENTIFIC OBJECTIVES

Because it lacks spectral resolution, an XUV monitor cannot provide data suitable for the derivation of the physical properties of the plasma in the solar atmosphere. Higher temperature features ($> 10^5$ K) can be distinguished from chromospheric features with an appropriate filter, however, and bright features can be distinguished from fainter features using integration times of different duration, enabling an observer to identify many structural details and to study their variation with time.

An XUV monitor will permit visualization of magnetic arch structures and provide continuous observations over the preflare pahse of a number of flares. With spatial resolution fine enough to resolve individual arches (< 5 arc-sec), and a temporal resolution of a few seconds, changes may be detectable in the arches of an active region about to flare, before and during the energy release. From these changes, it may be possible to draw some inferences about the plasma instabilities that are involved.

3.4.1 Flares

In Skylab observations, flares were found to originate in relatively small (20 to 40 arc-sec), individual magnetic arches in active regions. An illustration of this is shown in Figure 3-7 for the flare of June 15, 1973. Adjacent arches in an arcade of arches were often triggered sequentially, their footpoints developing into the double ribbon seen in Hα. Temperatures to above 2×10^7 K have been identified in spectrally separated XUV line flare images. These temperatures are reached in a small cloud near the top of the arch. The cloud, and a bright core within it, 5 to 10 arc-sec in size, continues to heat, then cools and fades 2 to 4 min after the onset of X-ray emission, showing major changes more rapid than could be followed with the time resolution available. No preflare observations were recorded from which the changes in a magnetic arch immediately before the onset of a flare could be determined.

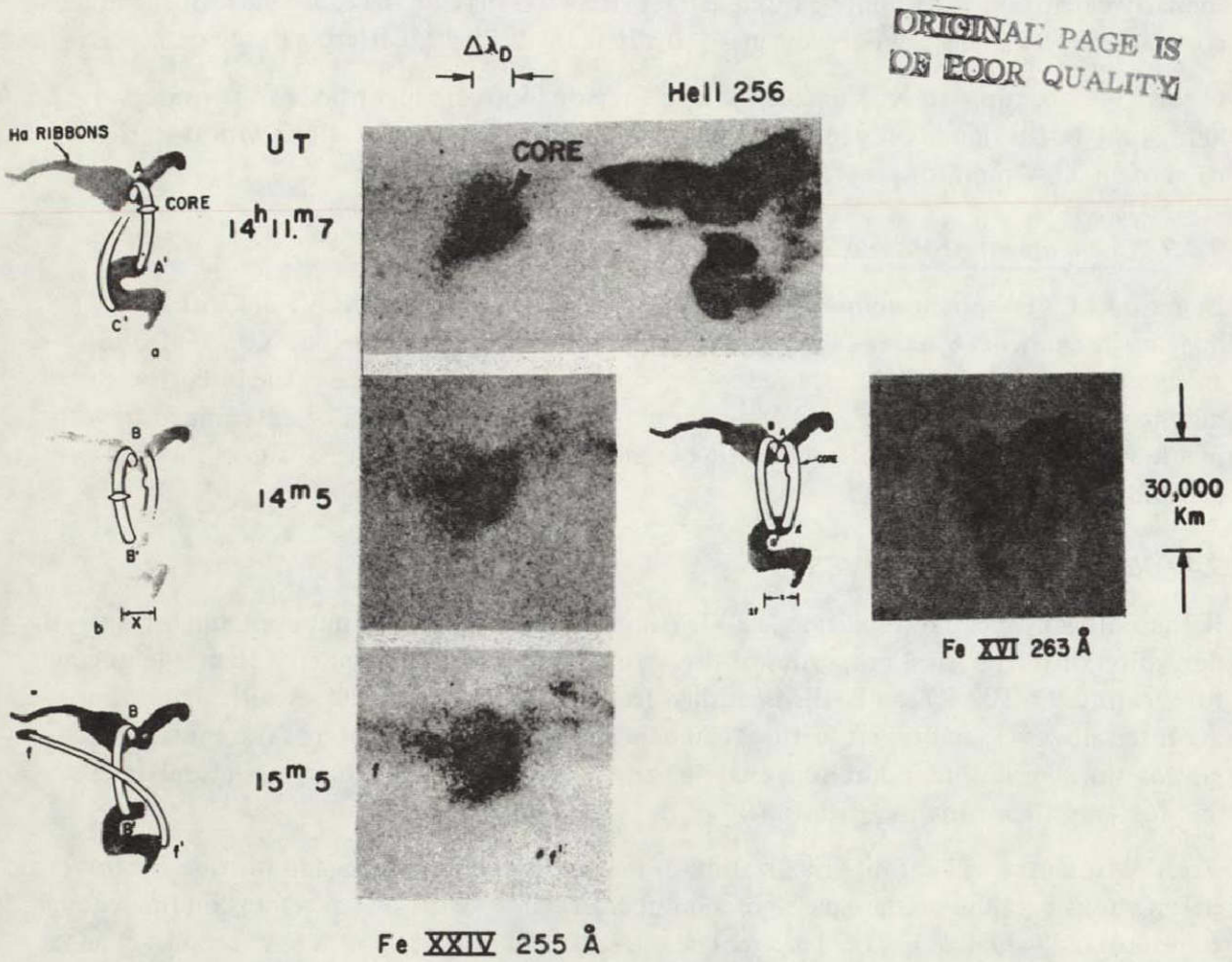

Figure 3-7. Small, Individual Magnetic Arches

Seen in XUV emission from material at transition-zone and coronal temperatures, the overall pattern of magnetic arches in an active region can persist for days, accommodating gradually to new emerging flux over a period of hours. At a temporal resolution of 90 sec, individual arches can sometimes undergo dramatic changes in the brightness of the entire loop as well as tiny (2 to 5 arc-sec) points near the footpoints.

At low-sptial resolution (20 arc-sec), the Skylab astronauts saw a great increase in overall XUV brightness of an active region, on the order of an hour before a flare. Then, reducing the brightness of their TV display, they were able to eliminate all but the brightest one or two points. It was the alternating fluctuation in brightness of these points on the XUV monitor that led them to recognize this activity as a preflare cue.

3.4.2 Coronal Structure and Magnetic Field Reconnections

Long-lived coronal structures, such as coronal holes and interregion magnetic arches, can be seen with an XUV monitor. Their long-term evolution is related to the growth-and-decay cycle of magnetic fields in active regions, but short-term changes occur with the emergence and diffusion of new magnetic flux. By comparing simultaneously recorded photospheric magnetograms and XUV images, the relationship between emerging flux and reconnecting magnetic fields in the corona could be clarified.

3.4.3 Time Correlations

With a temporal resolution of a fraction of a second, XUV monitor observations over the impulsive phase of a flare could reveal the sites in the magnetic arch pattern from which impulsive bursts are emitted. The footpoints of flaring arches and the high-temperature ($> 15 \times 10^6$ K) core near their tops are currently considered to be the most likely sources of hard X-ray and microwave bursts and of broadband XUV bursts that induce sudden frequency deviations (SFD's) at the Earth.

3.4.4 Bright Points

X-ray observations have shown that the bright points in the network have a mean lifetime of about 8 hr. Of the hundreds that are distributed over the Sun at any given time, some are found to increase greatly in brightness for a few minutes. These small (5 to 20 arc-sec) bipolar regions are seen on an XUV monitor. These relatively simple magnetic regions and their associated polar plumes can be seen in the coronal hole at the pole in the Mg IX 368 image of Figure 3-8. Their evolution and "flaring" could be studied and compared with that in the more complex magnetic patterns of flaring active regions.

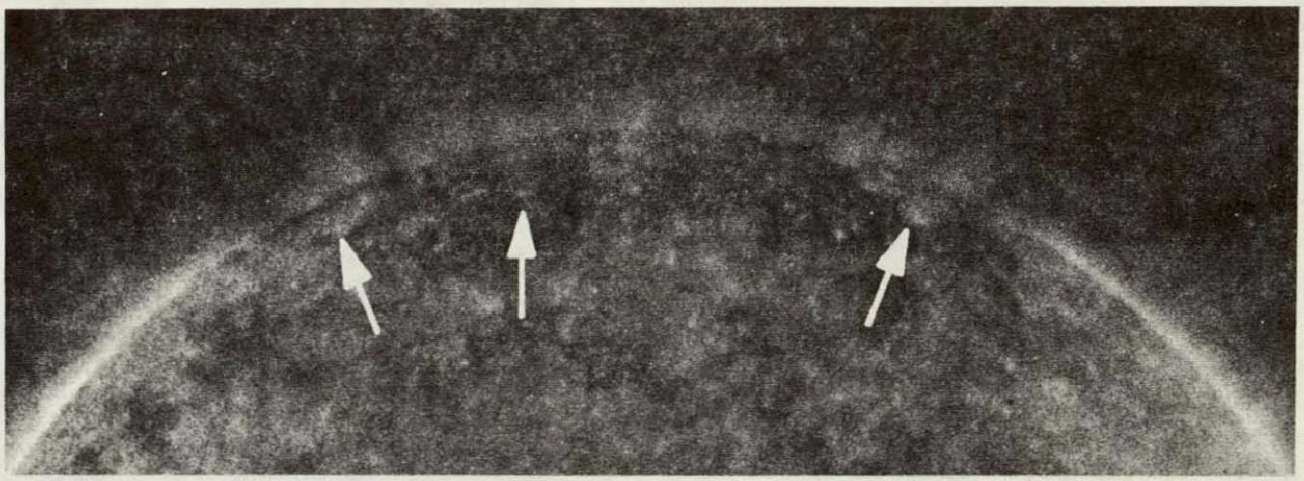

Figure 3-8. Small Bipolar Regions and Polar Plumes

3.4.5 Mass Motions

Surges, sprays, and eruptive prominences can be seen in the XUV. Figure 3-9 shows the event of January 17, 1974, in He II 304 Å and Fe XV 284 Å, as recorded by the ATM XUV Spectroheliograph. The two images, taken simultaneously, show material in the corona at chromospheric and coronal temperatures. The event was also seen on the XUV monitor. Such events are not only activated by flares, where they can carry away amounts of energy comparable to that released as radiation, but they have also been found to accompany long-duration soft X-ray enhancements (GRF's). This is illustrated in Figure 3-10, in He II 304 Å. Observations with an XUV monitor may clarify the heating and accelerating mechanisms of such motions.

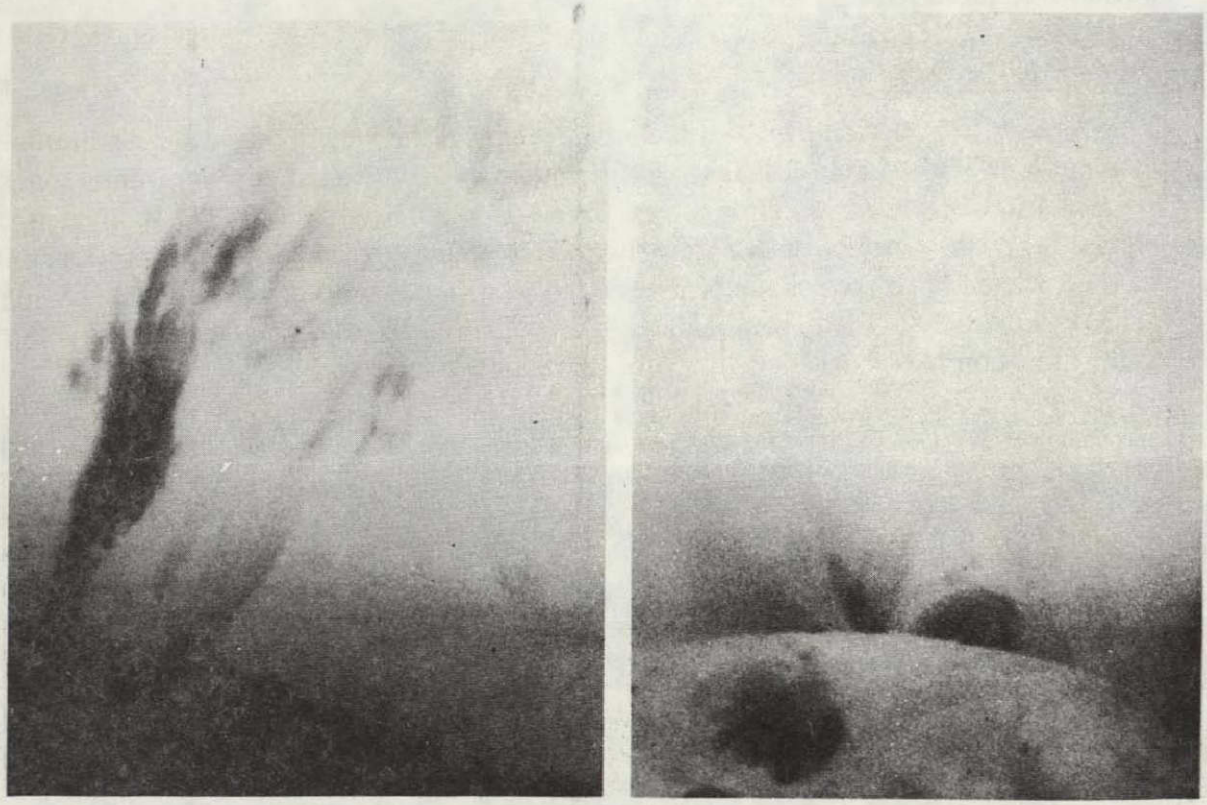

Figure 3-9. Eruptions of January 17, 1974, in He II 304 Å and Fe XV 284 Å

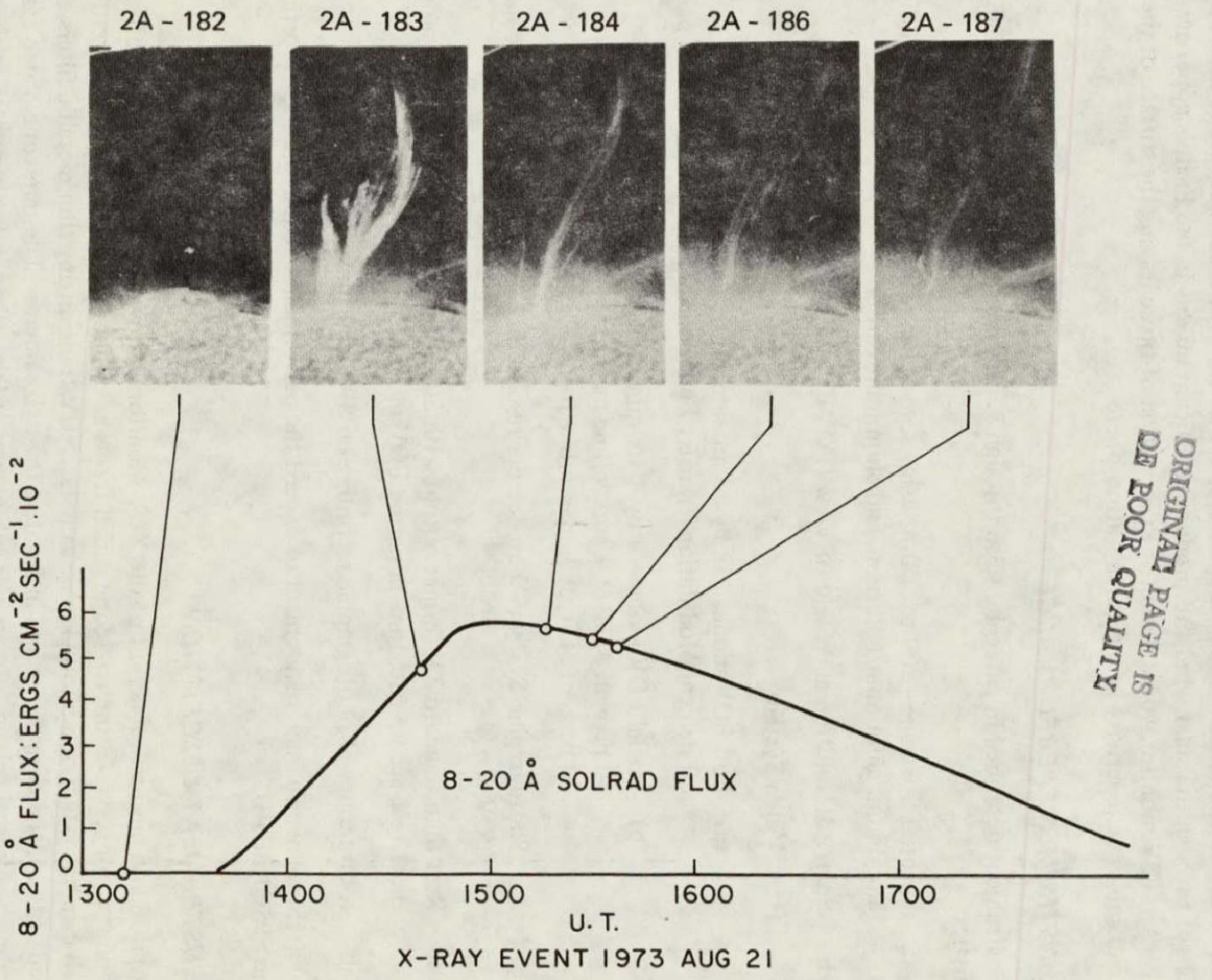

Figure 3-10. X-ray Event of August 21, 1973

3.4.6 Solar-Terrestrial Effects

Figure 3-11 shows a composite of an eruptive prominence, seen in He II 304 Å, and its extended effects in the outer corona. A small fraction of the eruptions that escape the Sun travel out through the solar wind and produce significant effects in the Earth's upper atmosphere. An XUV monitor would permit the correlation of those leaving the surface of the Sun and subsequent activity in the Earth's atmosphere.

3.5 INSTRUMENT PERFORMANCE

The instrument described in paragraphs 3.6 through 3.9 has the following performance characteristics:

a. Spectral Coverage - 200 to 600 Å, using several broadband XUV filters, including aluminum, aluminum/tellurium, and aluminum/carbon

b. Spatial Resolution and Field of View (FOV)

   1. Video System

      (a) Full FOV mode: 33 by 33 arc-min FOV;
      80 percent Modulation Transfer Function (MTF) at 8 arc-sec/line pair

      (b) Partial FOV mode: 4 by 4 arc-min FOV;
      50 percent MTF at 4 arc-sec/line pair,
      30 percent MTF at 3 arc-sec/line pair

   2. Photographic System - 2 arc-sec per resolution element pair with 41 arc-min FOV

c. Real-time standard TV format output with 20-sec up-date time in full FOV mode and 1 to 2 sec up-date time in partial FOV mode

d. 1300 frames of photographic recording on SWR roll film

These performance characteristics meet or exceed the performance requirements set forth by the SPSQRSP FDT.

3.6 INSTRUMENT DESCRIPTION

The optical and mechanical layout of the XUV Monitor is shown in Figure 3-12. An off-axis parabolic mirror serves as the telescope which forms a 2.5-cm diameter solar image on either a video camera system or a photographic camera. XUV transmitting thin metallic filters are located at the entrance aperture and in front of the two cameras. The telescope, video camera, film camera, filter wheel, and electronics subsystems are described in further detail in the paragraphs 3.7 through 3.11. The instrument canister/optical bench consists of 2.5-cm thick aluminum-honeycomb panels assembled in a rectangular configuration. Overall dimensions are 50 by 50 by 293 cm and the total weight is 125 kg. Structural rigidity is such that the first mode resonant frequency is above 50 Hz. The instrument is balanced and can be CG

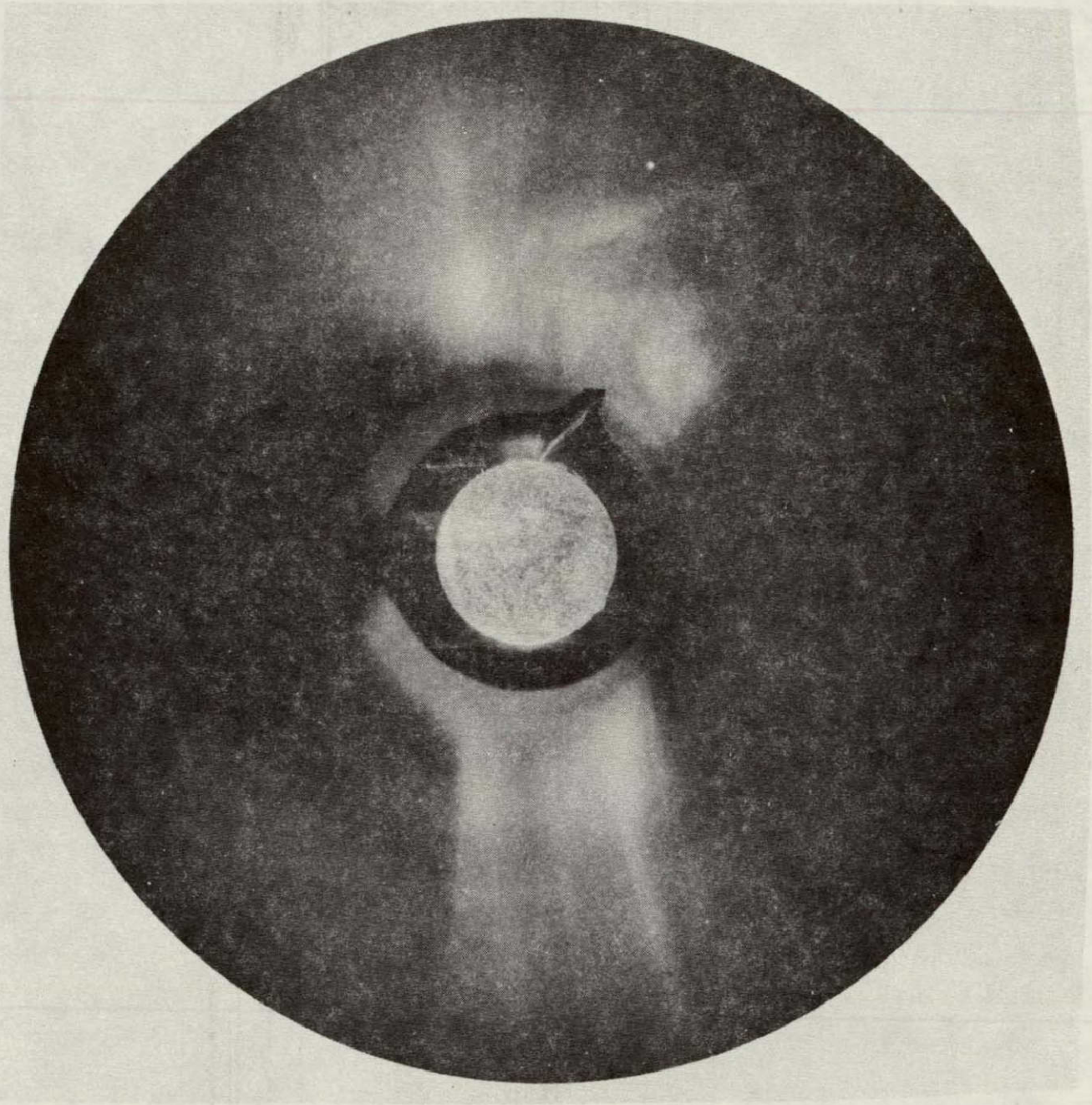

Figure 3-11. Eruptive Prominence in He II 304 Å

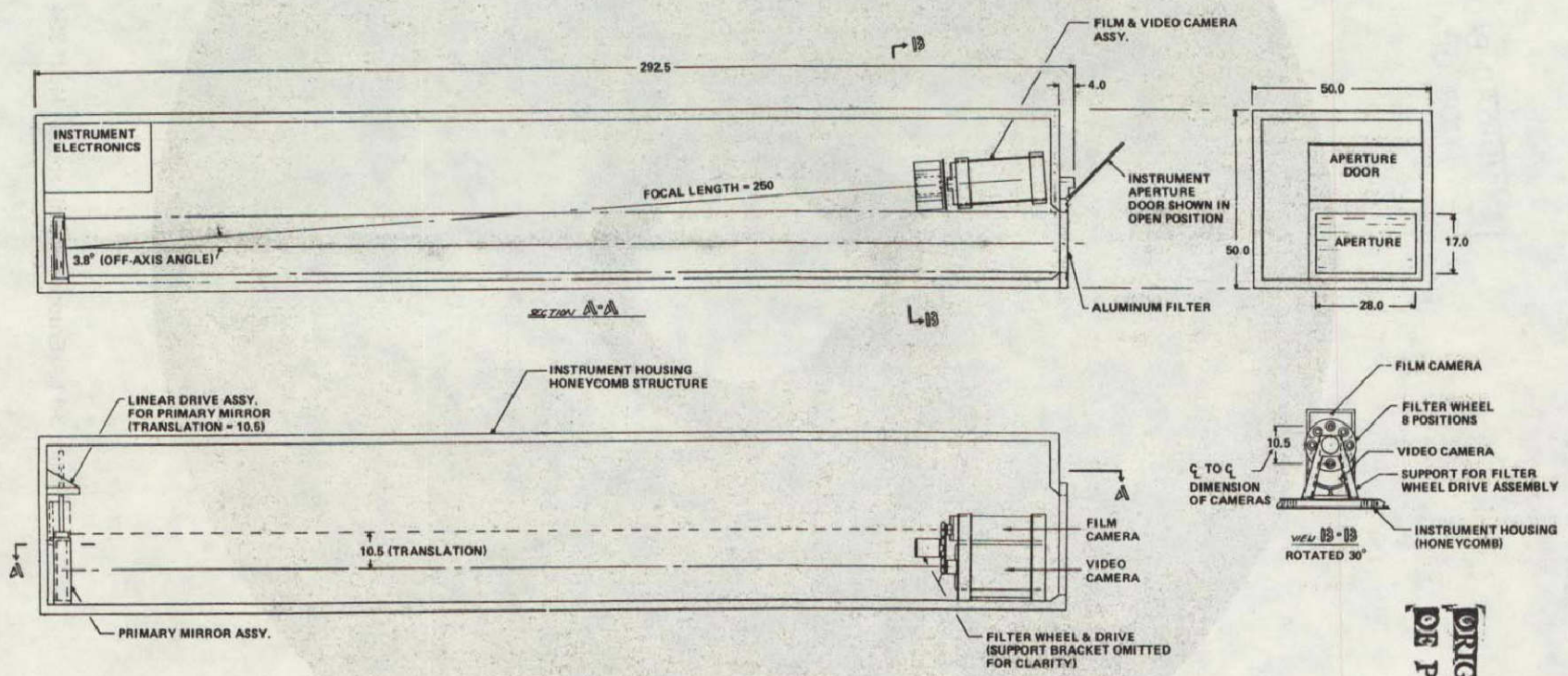

Figure 3-12. XUV Monitor for Spacelab Support Telescope

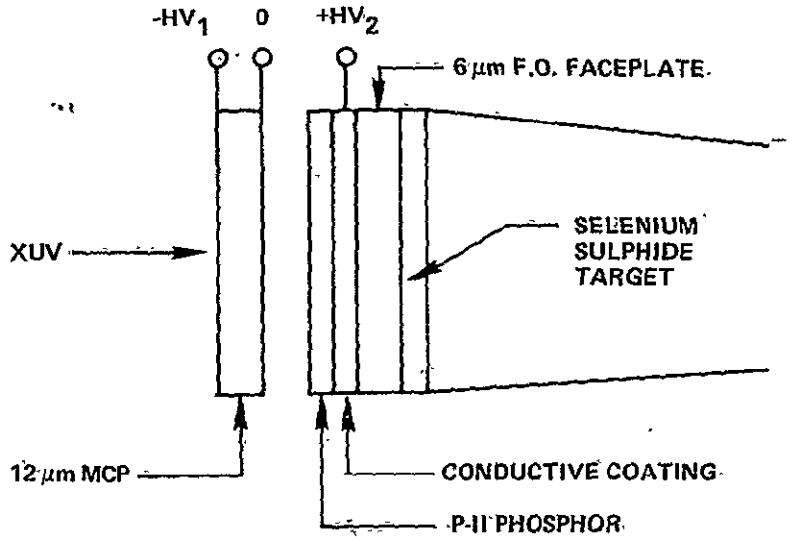

Figure 3-13. The Video Camera System

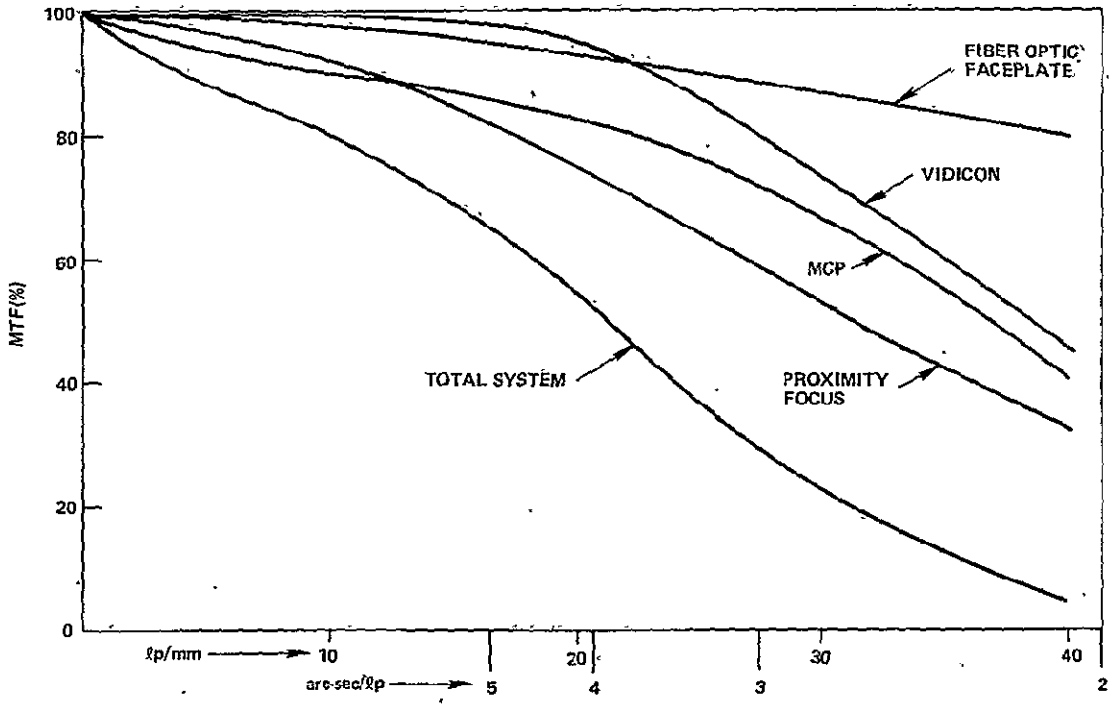

Figure 3-14. Video System Modulation Transfer Function (MTF)

The analog output of the camera will be processed to provide both a standard TV format output and a Spacelab compatible digital output. Recording of the video information can be carried out in the format most compatible to the mission. Figure 3-15 illustrates the basic video processing circuitry.

The video camera system operates in two modes: full field-of-view (FOV) and partial field-of-view. In the partial field-of-view mode, the microchannel plate is masked so that only the central 4 by 4 arc-min area is illuminated. In addition, the camera sweep circuitry is set so that only the central 256 by 256 pixels are read out. The analog output is converted by an A/D converter and stored in a 256 by 256 by 8 bit memory. This memory is then read out at a standard TV format rate, converted by a D/A converter, and sent directly to the Spacelab video display system. The small sweep format permits picture updating at the rate of 0.25 sec plus exposure time.

In the full field-of-view mode, no mask is placed in front of the microchannel plate and the camera sweep circuitry is set so that 2000 by 2000 pixels are read out. In addition, the A/D output is first routed through an averaging buffer and then to the memory. The averaging buffer averages together 8 by 8 blocks of the 2000 by 2000 pixel input and outputs a 256 by 256 pixel format. The picture updating rate in this mode is 16 sec plus exposure time.

In both modes the Spacelab video display system will be fed 256 by 256 pixels, i.e., the interlaced scan lines of the video monitor will not be used. Consequently, the video display system will not significantly degrade the data.

3.9 FILM CAMERA

The film camera holds 52 m of 35-mm wide Kodak type 101 and 104 film. This provides 1300 frames, each 40 cm wide. The film is transported from a supply spool to a take-up spool, each 10 cm in diameter, by means of a small dc motor. A focal plane shutter controls the exposure time of each frame. The complete camera measures 7 by 10 by 24 cm and weighs 6 kg. This camera design is based on an existing flight-proven roll film camera developed at the Naval Research Laboratory.

3.10 FILTER WHEEL

An eight-position filter wheel is located in front of the video and film cameras. Four positions are used for each camera. These four positions contain one aluminum filter, two aluminum/tellurium filters, and one aluminum/carbon filter. The three different filters provide different bandpasses in the 200 to 600 Å range as illustrated in Figure 3-16 and are arranged so that the same filter type is positioned in front of the video camera and film camera at the same time. A 45-deg stepper motor drives the filter wheel mechanism, which is based on a proven mechanism used on the ATM instruments.

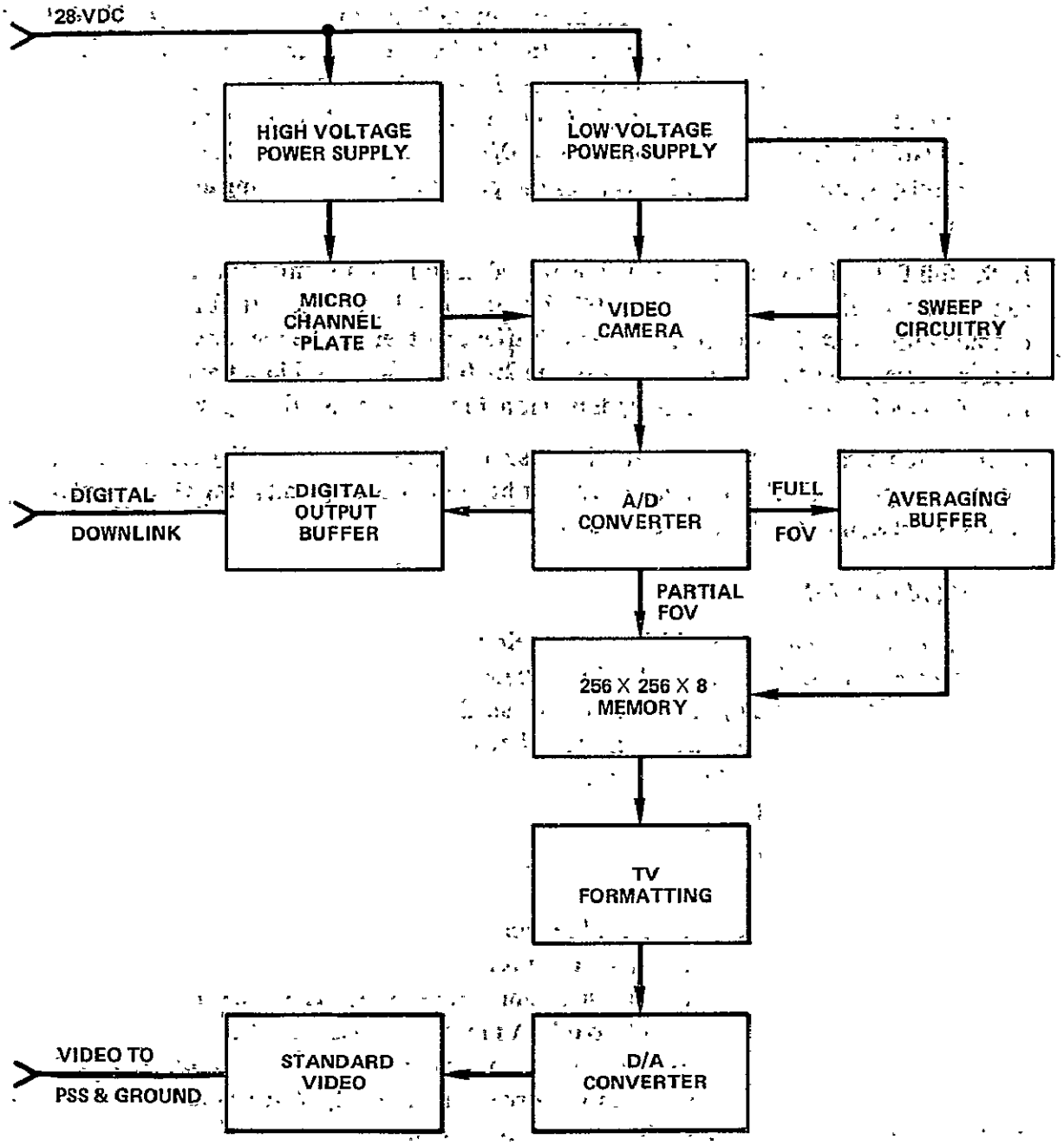

Figure 3-15. Block Diagram of the SST XUV Monitor Video System

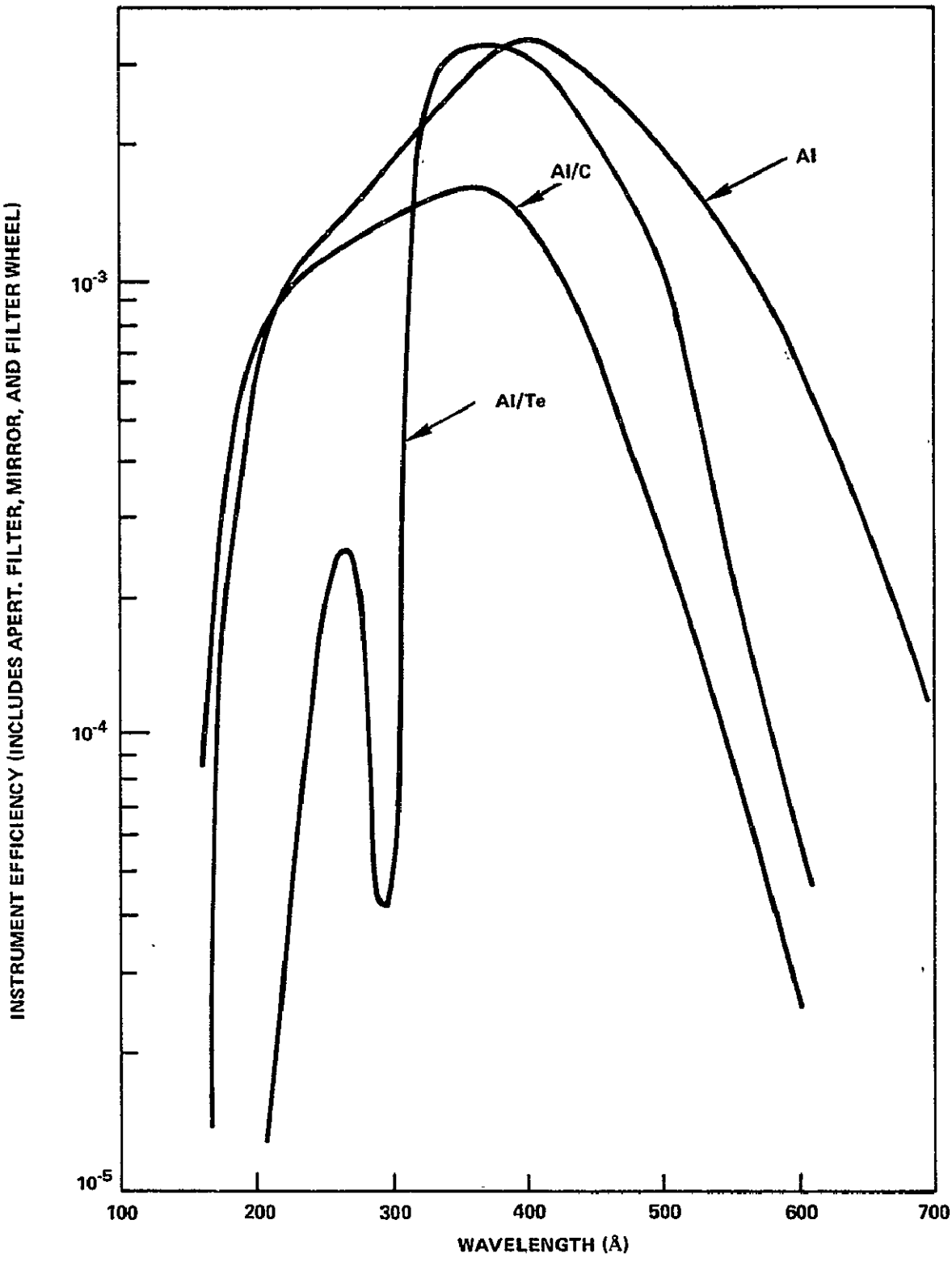

Figure 3-16. Effect of Filter Combinations on Instrument Bandpass

3.11 ELECTRONICS

Figure 4-17 illustrates the basic layout of the XUV Monitor electronics. With the exception of the video system explained earlier, the electronics are limited to power, drive, and monitor functions. Sequencing and timing of the XUV Monitor will be handled by the Spacelab Experiment Computer. In addition, input/output (I/O) signals pass directly to the Remote Acquisition Unit (RAU). No input command decoding or output multiplexing is necessary within the instrument. Seventeen discrete commands are necessary to operate the XUV Monitor and are listed below:

• MCP HV Adjust	4
• Filter Wheel Advance	1
• Video Camera Mask (In/Out)	2
• Mirror Position (Video/Film)	2
• Film Camera Shutter (Open/Close)	2
• Aperture Door (Open/Close)	2
• Field of View (Full/Partial)	2
• Power (On/Off)	2
Total Commands	17

3.12 OBSERVATIONAL MODES

The XUV Monitor operates in three observational modes:

- Real-time, full-disk video display
- Real-time, partial-disk, high-resolution video display
- Full-disk photographic recording

The real-time, full-disk video display mode will permit the payload specialist to survey the entire Sun. In this mode, the XUV monitor can aid in instrument coalignments and pointings, and, at the same time, record large-scale feature development on the Sun. Video updating in this mode is 16 to 20 sec.

When more detailed feature observation and pointing is required, the XUV Monitor can be switched instantly to the real-time, partial-disk video display mode. This mode provides an enlarged video display of the central 4 by 4 arc-min region with high spatial resolution and can be used for high-precision feature pointing and real-time observation of transient events. Video updating in this mode is 1 to 2 sec.

At any time, the instrument can be switched to the photographic mode (1 to 2 sec switchover time) and a full-disk image of the Sun will be recorded using the same filter type as that presently in front of the video camera.

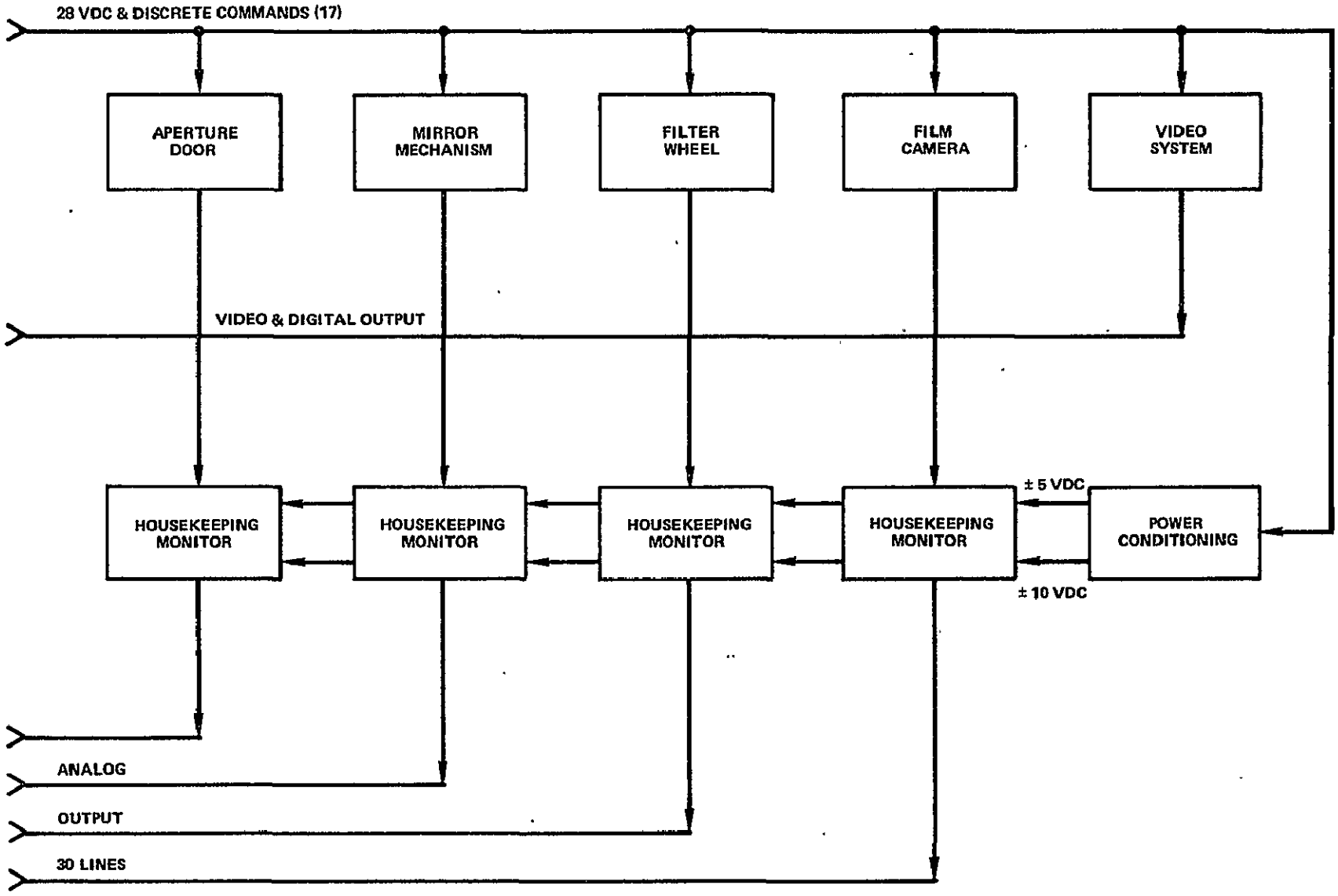

Figure 3-17. Block Diagram of the SST XUV Monitor

SECTION 4

SHORT WAVELENGTH SPECTRAL IRRADIANCE MONITOR

ACKNOWLEDGMENTS

This report was prepared by R. L. Blake of the Los Alamos Scientific Laboratory. Much of it has been pieced together from information provided by individuals some of whom actually furnished copies of proposals they had submitted for monitor experiments. J. Bartoe and G. Brueckner of U.S. Naval Research Laboratory provided the system for 120 to 400 nm measurements. K. A. Anderson and his colleagues from Berkeley and elsewhere provided the CEMA monitor scheme for 2 to 200 nm measurements. R. Moore of Cal Tech wrote an initial report emphasizing flare monitoring. J. Beckers of Sacramento Peak Observatory and R. Blake of LASL conceived the pin-hole and broad-band monitor technique. C. J. Wolfson contributed to editing the revisions. A good deal of the performance requirements has been extracted from preliminary drafts for the book, "The Solar Output and Its Variations," edited by O. R. White.

4.0 *SHORT WAVELENGTH SPECTRAL IRRADIANCE MONITOR*

4.1 *INTRODUCTION*

This report contains the preliminary ideas for a Space Shuttle monitor of the solar subvisible spectrum as a potential special purpose experiment that could provide a data base for a wide range of studies in solar-terrestrial physics. For brevity, we shall refer to the subvisible solar spectrum from 0 to 400 nm as the XUV. This extends the accepted nomenclature without harm. We present the scientific uses, the performance requirements, and conceptual outlines of possible instrumentation.

Observations of the solar XUV spectrum are important to solar physics, aeronomy, and climatology. Solar physics needs include the following:

- Calibration crossreference for Solar Physics Spacelab prime experiments that observe in the XUV
- Broad range coverage of the solar spectral irradiance to provide adequate boundary value data for models of the processes responsible for heating the outer solar atmosphere and the solar activity cycle
- The same boundary value data for solar flares, in order to establish the energy content of flares and provide rough criteria for specifying the relative contributions of competing processes in the buildup and release of flare energy
- Provide real-time information on solar activity for possible control of prime solar experiments
- Provide correlative data to other solar physics investigations in space or on the ground, to experiments pertinent to solar-terrestrial phenomena, and to statistical studies

Some needs for an XUV monitor in atmospheric sciences, aeronomy, and climatology include the following:

- An accurate monitor of the 200 to 300 nm portion of the solar flux, which makes a significant contribution to the solar constant
- High resolution (0.002 nm) occasional monitoring of the O_2 absorption band region 175 to 204 nm for atmospheric modeling
- Moderate resolution (0.1 nm) monitoring of the XUV region 0.1 to 300 nm for atmospheric modeling
- High-time resolution ($\sim$ 1 sec) XUV monitoring 0.1 to 300 nm for ionospheric modeling

- Long-term monitoring to permit evaluation of the relative roles of XUV, solar wind, solar flare protons, and galactic cosmic rays to atmospheric processes—especially processes with long-time constants such as the NO_x cycle and ozone variability.

4.2 SOLAR PHYSICS

4.2.1 Calibration of Other XUV Experiments

Some of the most informative observations of solar flares from the Skylab missions were soft X-ray filtergrams and EUV spectraspectroheliograms recorded on photographic film. Presumably, similar observations in the XUV will be obtained with instruments on the Shuttle sortie and free-flyer missions in the future. Photographs are excellent for recording the spatial structure of flares, but it is difficult to accurately measure absolute intensities, especially if the film becomes saturated in some parts of the flare. In this connection, it would be very useful to have an independent measure of the total flux from the flare in that portion of the spectrum recorded by the photograph. These observations could be obtained with an XUV flux monitor with appropriate spectral selectivity. Experience has shown that even good photoelectric detectors are subject to gradual changes in calibration with time. Repeated flights of calibrated XUV flux monitors would serve to recalibrate these as well as film.

For flare and nonflare observations, a record of the total output of the Sun in the spectral band of interest would be a convenient check on the calibration of any solar experiments in orbit. Such a record would also provide an independent measure of the integrated effect of large scale features such as coronal holes or extended old plage regions, as well as active regions, especially if the XUV monitor has some spatial resolution.

4.2.2 Nonflaring Sun Irradiance

The solar spectrum shortward of 300 nm contains radiation emitted from all the constituent parts of the observable solar atmosphere: photosphere, temperature minimum, chromosphere transition-region corona, and active-region corona. In general, the shorter the wavelength, the greater the temperature of the source of emission in the solar atmosphere. For temperatures above 10^4 K, essentially all of the emission is contained in the XUV spectrum shortward of about 200 nm. Thus, with sufficient spectral resolution, observations of the XUV spectral irradiance allows the radiative output of the entire solar atmosphere to be measured as a function of temperature above 10^4 K. Such measurements would provide a basic empirical test for models of the solar atmosphere, both for quiet regions and for active regions.

Because the solar atmosphere is perpetually changing, models must be time dependent both for the Sun and the terrestrial phenomena influenced by the Sun. The radiation flux and solar wind are the primary measurable parameters available, from which we must attempt

to understand the nature of the Sun, its changes, and terrestrial effects—of which there are many. To date, the lack of a continuous solar XUV data base has precluded answers to some important solar and terrestrial questions.

4.2.3 *Flares*

4.2.3.1 *Total Energy.* A quantity fundamental to the understanding of any physical phenomenon is the total energy involved in the phenomenon. In solar flares, all of the energy that is not carried away by mass motions, such as ejections or blast waves, must eventually be radiated away. It appears likely that less than half of this contained energy is radiated in the visible.[2 and 3] Therefore, it is essential to measure the total XUV flare output in order to measure the total energy of a flare.

4.2.3.2 *Thermal Component.* Spectral observations of soft ($\lambda > 0.1$ nm) X-rays from flares show that flares generate thermal plasmas that can be approximated by isothermal models with temperatures of the order of 10^7 K. The thermal energy content at any instant is given by

$$Q_{th} = 3kTn_eV, \tag{1}$$

where V is the volume of the thermal X-ray plasma. The shape and magnitude of the thermal X-ray spectrum, respectively, determine the temperature T and the emission measure $H \equiv n_e{}^2V$ of the thermal X-ray plasma. Hence, for given observed values of T and H, the thermal energy content is inversely proportional to the electron number density n_e:

$$Q_{th} = 3kT\frac{H}{n_e}. \tag{2}$$

The electron number density is uncertain by about a factor of 10. Consequently, it is desirable to measure the total XUV output of the thermal flare in order to determine the total thermal energy to better than a factor of 10.

Observation of the XUV spectrum of the thermal flare could help to determine the relative importance of conduction cooling and radiative cooling of the thermal X-ray plasma. The calculations of Tucker and Koren[4] show that at temperatures in the vicinity of 10^7 K and above, for a plasma of coronal composition, more than 80 percent of the emitted radiation is at wavelengths shortward of 2.5 nm. Therefore, observation of much less energy in the XUV spectrum longward of 2.5 nm than shortward would imply that radiative cooling dominates, and vice versa.

4.2.3.3 *Impulsive Component.* The rapid rise of the soft X-ray thermal component during the early part of the flare is often accompanied by an impulsive burst of hard ($\lambda < 0.1$ nm)

X-rays. Estimates of the energy content of the high-energy ($\gtrsim$ 10 keV) electrons that produce the hard X-rays indicate that these electrons contain as much energy as the thermal plasma at thermal X-ray maximum.[5] This suggests that the impulsive hard electrons may be the energy source for the thermal flare. On the other hand, estimates of the total XUV flux from observations of the ionosphere indicate that the XUV emission during the impulsive phase is about equal to the energy content of the hard electrons.[6] This suggests that most of the energy of the hard electrons may be immediately radiated away rather than going into the thermal X-ray plasma. XUV observations of moderate accuracy are required for both the impulsive and thermal phases in order to determine the amount of thermal energy for comparison with the energy available from the hard electrons.

We have cast this discussion in terms of an electron stream model. The need for XUV spectral measurements is equally relevant to thermal models since the spectral energy content and time history are crucial parameters in the evaluation of any model.

4.2.4 *Real-time Data*

Real-time information on solar activity available from XUV monitors is important not only to solar physicists but also to other segments of our society. Pilots of high-flying aircraft have to guard against accumulated overdoses of radiation experienced when cosmic-ray flares coincide with their flights. Power companies frequently encounter short circuits during flare-induced geomagnetic storms. Geophysical prospecting with magnetometers is unreliable during solar-induced geomagnetic disturbances. And so on. The various interests in real-time monitoring have, to date, been partially satisfied by NRL and NOAA satellites, Solrad, and SMS-GOES respectively. The monitor system described herein augments the present Solrad and SMS-GOES systems by additional wavelength coverage and resolution as well as an attempt to standardize and calibrate for improved accuracy.

Real-time information on solar conditions, as revealed best by XUV radiation, is important to solar physicists for control of rocket launches and prime solar experiments on the Shuttle. Experience with ATM pointed up the vital importance of real-time control to obtain critical observations.

4.2.5 *Correlative Data*

Solar activity is physically linked by XUV and particle emissions to a wide variety of solar-terrestrial phenomena. Data from many ground-based and space experiments are compiled and distributed by NOAA. These data have been used extensively by a large fraction of the solar-geophysical community for research and for correlative studies. The XUV monitor data that we suggest here would provide an expanded data base that would permit new and improved analyses of solar-terrestrial phenomena.

4.3 *AERONOMY AND ATMOSPHERIC SCIENCE*

In recent years we have learned that important variations in the Earth's biosphere arise from interactions of the near-surface environmental system with a far more extended system extending out to the Sun. Not only does solar radiation drive the circulation of the lower atmosphere with its weather patterns, but the short wavelength XUV portion is responsible for conditions in the high atmosphere well above the weather-dominated layer. These higher portions contain trace constituents whose importance far exceeds their fractional concentration, a prime example being ozone. The concentrations and changes in these trace constituents caused by fluctuations in the solar XUV spectrum must be assessed as a baseline to compare with changes caused by man's technologies. Solar emissions related to the 22-year solar activity cycle cause major changes in Earth's magnetic field, plasmasphere, upper atmosphere, and ionosphere. In turn, there are induced effects at Earth's surface with significant socio-economic consequences.

Examples include corrosion in the Alaska pipeline, disruption of telephone and radio communications, and others mentioned earlier. There are numerous indications that changes in Earth's climate, and possibly even global weather patterns, are related to solar activity in spite of the small fraction of the solar output contained in XUV and the solar wind and flare emissions. For example, drought conditions in the United States high plains have occurred in association with minimum conditions in the 22-year solar activity cycle regularly since the mid 1800's,[7] and with longer term solar activity minima for the past 5000 years (where comparison has been possible[8]). At present there is insufficient basic knowledge of climate, the upper atmosphere, magnetosphere, and the Sun as an interacting system to permit definitive conclusions on cause-effect relationships. The XUV monitor for Space Shuttle will expand the knowledge base about this total environment so that realistic assessments can be made about consequences to the natural environment from man's technologies and vice versa.

4.3.1 *XUV Contribution to Solar Constant*

Climatologists and atmospheric scientists estimate that a one percent change in the solar constant could produce a significant change in climate and weather patterns. Because there are numerous competing processes that control the atmospheric circulation in a nonlinear way and the dominant thermal forcing factors are themselves not accurately known, it is premature to expect profound climatic predictions related to small solar constant changes. But it is not too soon to start improving our knowledge of the solar spectrum and its variations, because statistical studies are now sufficiently compelling to force admission that the weather and climate are related to the solar activitiy level regardless of the small amount of energy that may be attributed to transient solar processes.[7,8,9] Observations and models reveal that coupling occurs between adjoining atmosphere levels as a consequence of turbulence mixing, diffusion, gravity waves, ion drag, and electrical conductivity from surface to upper atmosphere, to name but a few processes. Processes that couple various portions of the terrestrial atmosphere are being studied on the hypothesis that they provide the

mechanism for Sun-weather relations. Attempts to sort out the mechanisms linking solar activity to weather and climate will be assisted by improved XUV monitoring.

About one percent of the solar constant is contributed shortward of 300 nm, with about 0.01 percent from below 200 nm. Thus, the 200- to 300-nm range is the only portion significant to the solar constant which can, in the near future, be measured to 0.1 percent accuracy from space.

4.3.2 *XUV Monitoring 0.1 to 300 nm*

It is important to compare variations in the observed solar radiance shortward of 200 nm with any observed changes in the solar constant, as this could give clues to the physical cause of the change. Moreover, Earth's mesosphere, ionosphere, and magnetosphere owe their entire existence to XUV and particle emission containing only 0.01 percent or less of the solar output. Solar radiation absorbed from about 200 to 300 nm is responsible for the presence of the stratosphere. Absorption of this radiation, mainly by ozone, causes the temperature increase with height, which stabilizes the stratosphere against free convection. Radiation shortward of 242 nm dissociates diatomic oxygen, which is the first step in the ozone formation process. In the O_2 absorption bands from 175 to 204 nm, the need for high-resolution monitoring is greatest (0.002 nm).

Solar XUV flux between 1 and 300 nm is entirely absorbed in the terrestrial atmosphere over a wide range of altitude. The energy balance in all regions above the troposphere is determined by this absorbed XUV solar energy flux. There are indications that the solar XUV is variable by 5 percent or more[10] in the continuum below 210 nm. At shorter wavelengths, the variability increases until at 0.1 to 1 nm it reaches several orders of magnitude and the high-energy flux below 0.1 nm only appears during some flares. Flux variability below 200 nm may arise, in part, from processes in the undisturbed solar atmosphere. Certainly it arises, in large part, from the growth and decline of centers of activity. This is evidenced by observed changes with solar rotation as active regions appear and disappear from view, and with the solar activity cycle as the number of active regions grows and declines. Models of the terrestrial upper atmosphere must account for daily, monthly, seasonal, and solar-cycle changes.

The ability to answer questions about such factors as SST exhaust effects and halocarbon (spray can) effects depends critically on two factors. One is improved knowledge of trace constituents in the upper atmosphere, and the second is improved knowledge of the solar radiation input, both its spectral irradiance and its variability.

4.3.3 *High-time Resolution Monitoring*

Solar flares provide an impulsive excitation of the ionosphere that permits study of the transient response on time scales at least as short as 1 sec. Such studies are important, not only to complete the development of quantitative practical relations between the flare-radiation flux and various types of observations of the flare-induced Sudden Ionospheric

Disturbances (SID), but also to accurately examine the physical relation between the solar radiation and its consequent ionospheric effects. For moderate and high levels of solar activity, there is evidence of a conflict of about a factor of 2 between the measured ionospheric electron density N_e and temperature T_e, and the corresponding values computed with solar flux measurements, a model atmosphere, and laboratory measurements for ion-chemistry reaction rates.

Measurements of the spectral XUV flux $\Phi(\lambda, t)$ from solar flares provide a unique opportunity for studying the relationship between the solar XUV radiation and SID. Consider the electron continuity equation:

$$\frac{dN_e(h,t)}{dt} = \underset{\text{Production rate}}{q_e(h,t)} - \underset{\text{Ion chemistry loss}}{\alpha_{eff}(h)\,N_e^2} - \underset{\text{Transport}}{\nabla\,(\vec{v}N_e)} \qquad (8)$$

where the photoionization plus secondary ion production rate q_e (ht,) is proportional to the solar radiation flux $\Phi(\lambda, t)$ and $\alpha_{eff}\,N_e$ is equivalent to the sum of the constituent ion densities weighted by their corresponding electron recombination rates.

Using the rise of a very impulsive XUV burst, one can examine the relation between Φ and dN_e/dt (h, t) at E- and F1-region altitudes (h) where photoionization and secondary ionization processes are dominant, ion-chemistry processes are minor, and transport processes are negligible. At the end of a rapid decay XUV burst, dissociative electron-ion recombination processes dominate at E and F1 region altitudes and transport processes dominate at F2 region altitudes. In other words, the transient effect of impulsive flare emission permits one to partially separate the ionospheric physical processes. This cannot be done in the quasiequilibrium studies of nonflare conditions.

Attempts to conduct such studies during the past decade have not succeeded because solar flux measurements lacked sufficient wavelength coverage. No solar flare has ever been observed over the full wavelength range of interest. On the other hand, the wavelength coverage and the time and spectral resolution of the measurements suggested for the XUV monitor here have been designed to satisfy the ionospheric physics requirements. Recent studies show that such broad-band measurements are quite adequate for studying the ionospheric effects of flares.[11] The high sensitivity of the suggested measurements is also important since most solar flares produce relatively small perturbations both in the total solar XUV flux and in the ionosphere. Such small ionospheric perturbations have been accurately measured in the E and F1 regions, but previous broad-band solar-flux detectors did not have the necessary sensitivity and wavelength coverage to measure accurately the small perturbations in the whole-disk flux.

The study of the ionospheric effects of flares should include a set of flares ranging in intensity and time structures. Small flares produce small ionospheric perturbations where linear perturbation theory for the ionospheric response is appropriate, i.e., second order perturbation terms are negligible. At the same time, it is highly desirable to observe the very large XUV bursts that occur only about once or twice per year. Such large bursts produce substantial enhancements in ionospheric electron temperature and induce large variations in the ionospheric currents and Earth's magnetic field.

4.3.4 *Long-term Monitoring*

There is a need both in meteorology and aeronomy for long-term monitoring of solar XUV at least over a solar cycle. As mentioned earlier the solar XUV and particle emissions comprise a very small fraction of the energy responsible for thermal forcing of the troposphere, yet the statistical studies show that these emissions do influence the weather and climate. In order to quantitatively evaluate possible interaction mechanisms, it will be necessary to have a reliable data base of XUV and particle emissions extending at least over a solar cycle.

In general, the aeronomical arguments given earlier apply here to the case of long-term monitoring, since there are evolutionary models of the upper atmosphere as well as instantaneous models. The evolutionary models will take on increasing significance to our whole society as man's inputs to the atmosphere in the form of CO_2, nitrogen oxides, radioactive releases, and hydrocarbons continue to accumulate. These inputs get caught up in complex cycles of interacting processes, whose consequences can be traced only if all the inputs are known accurately.

4.4 *PERFORMANCE REQUIREMENTS*

The XUV monitor instrument has to be designed with the following factors in mind:

- Both solar physics and aeronomy needs
- Wavelength resolution
- Time resolution
- Measurement accuracy
- Sensitivity
- Dynamic range

Consider the last factor. Table 4-1 represents our best estimtes from the literature and colleagues about solar flux measurements made to date. The wavelength intervals have been selected for solar physics reasons as illustrated in Figure 4-1. One can show by general arguments for hot-plasma emissivity that 75 percent or more of the flux from each of the designated wavelength intervals is emitted from regions of the solar atmosphere in the temperature range denoted in each λ range. Thus, we can crudely isolate components of

Table 4-1
Solar Flux and Variability*

Designation	X-Rays	Short XUV	Long XUV	Ly α	Cont.	Cont.	Cont.	Cont.	Ca II	Solar Const.
Wavelength (nm)	< 1	1-30	30-120	121.6	120-160	160-200	200-300	> 300	395	0 - ∞
Absolute Accuray of Measurements (%)	X 2	X 2	± 30	± 30	± 30	± 30	± 20	< 1	± 10	± 0.2
Flare Variability (importance 3)	X 100	–	–	+ 16	–	<+ 1	?	<+ 0.15	≈ + 0.5	< 0.1
Varibility of Slowly Varying Component (appearance of one major active region)	X 1 - X 100	< X 2	~ 20	15-30	–	> 0.5	?	–	< 5	< 0.03
Change Associated with Sunspot Number Change from 0 to 120	X 300	≳ X 2	< 100	30-50	–	3	?	< 1	< 15	< 1
Total Flux Change for 11-Year Moderate Solar Activity Cycle	X 500	≳ X 2	< 100	100	–	> 3	?	< 1	> 15	< 1

* Entries with X are a multiplicative factor and without X are percentages.

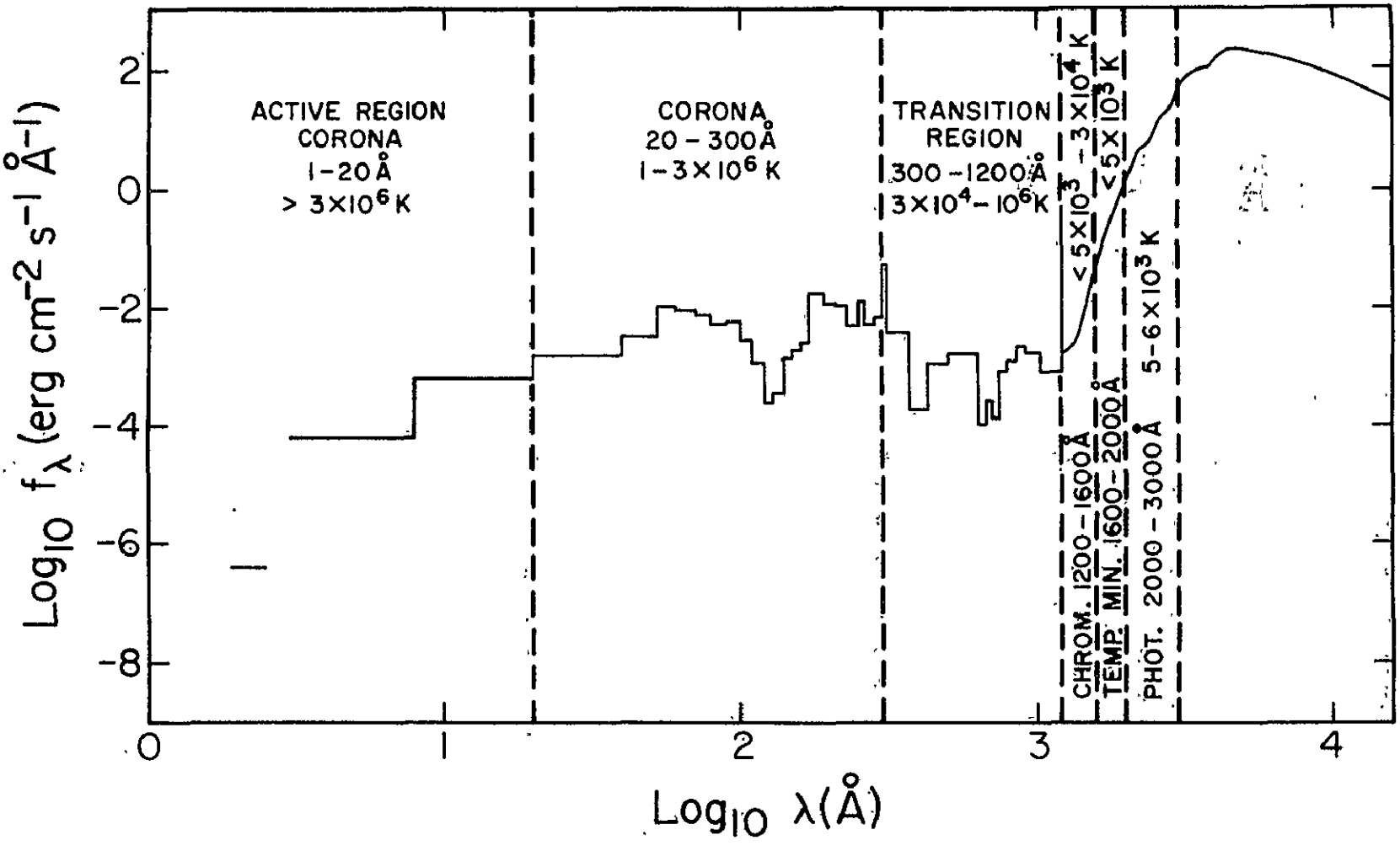

Figure 4-1. The Solar Spectral Irradiance

the solar atmosphere. Table 4-1 shows that X-rays short of 1 nm have been measured with an accuracy of about a factor of 2 and have been observed to vary by factors up to 500 over the solar cycle. As one moves to the right in the table, the observed variability decreases dramatically (note the first two columns specify multiplicative factors and the remaining columns show percentages). Two individual lines, Lyα and CaII H+K, are included along with bands of emission. It is clear that for X-ray observations a dynamic range $\gtrsim 1000$ is required, whereas only a factor of 2 is needed at the longest wavelengths.

Table 4-2 treats the other factors on the list as well as can be determined from the literature and discussions with colleagues, not all of whom will agree completely with Table 4-2. It gives the estimated near-future requirements on solar XUV flux measurements in order for improved models to be generated for the solar atmosphere on one hand and for Earth's atmosphere on the other hand.

Aeronomy needs for terrestrial atmospheric modelling include moderately high-spectral resolution ~ 0.1 nm with full spectra every few hours. The spectral resolution requirement arises from the large variations in photon absorption coefficients for atmospheric constituents. In the O_2 bands 175 to 204 nm the requirement is so stringent as to preclude the utility of a simple monitor. The need to assess man's influence on the upper atmosphere is expected to spur much improved measurements and models, which may impose an XUV flux accuracy requirement ~ 10 percent during the Space Shuttle era. Aeronomy needs during flares can be met with broad-band monitors, but high-time resolution ($\lesssim 1$ sec) is required along with high sensitivity. Flare-induced ionospheric transients have been observed to vary in times of 1 sec. Donnelly[11] has used ionospheric transients to deduce probable XUV fluxes from flares. His results for the impulsive phase of a typical sample of flares are shown in Figure 4-2. The upper curve is the nonflare whole-Sun XUV flux. The lower horizontal bars represent the additional contribution from the impulsive phase of a flare. The flare contribution above 1 nm (10 Å) is seen to be typically 100 times weaker than the quiet-Sun flux. Our sensitivity estimates for flare XUV monitors are based on Figure 4-2 and a similar model for the thermal flare component.

Longward of 120 nm we know only that the flare contribution is very small compared to the quiet-Sun total flux and very high sensitivity would be required. For example, very rare flares produce small patches of brightening in white light images from which one can estimate roughly that the sensitivity required is ~ 1 percent on a high-resolution image or less than one part per million of the whole-Sun flux. Such measurements are not appropriate for a monitor instrument.

Solar physics requirements for flare measurements are essentially identical to those for aeronomy if the wavelength intervals are approximate as used in the figures and tables. Solar constant measurements are only relevant above 200 nm. The range of 200 to 300 nm contains about 1 percent of the solar constant and may vary by a small amount (probably < 2 percent) over a solar cycle. Thus, a sensitivity $\lesssim 1$ percent is required to detect any variability and an accuracy of a few percent would assure the error in the total solar constant would be smaller than the accuracy (~ 0.1 percent) expected for total solar constant measurements.

Table 4-2
Performance Requirements for XUV Monitor*

Performance Category and Wavelength Interval (nm)	Scientific Discipline				
	Aeronomy		Solar Physics		
	Normal	Flares	Solar Constant	Solar Atmosphere	Flares
Wavelength Resolution					
0.1 - 175	0.1	0.2 - 20	–	0.2 - 20	0.2 - 20
175 - 204 occasional	0.002	–	–	–	–
175 - 204 monitor	0.1	20	–	0.1 - 20	20
204 - 300	0.1	20	2	0.1 - 20	20
Time Resolution					
0.1 - 120	hours	< 1 sec	–	hours	≲ 1 sec
120 - 400	hours	–	hours	hours	?
Absolute Accuracy					
0.1 - 120	10 - 20%	10 - 20%	–	20%	20%
120 - 300	10%	10%	10 - 1%	20 - 2%	20%
Sensitivity†					
0.1 - 2	–	< 0.1% FS	–	< 0.1% FS	< 0.1% FS
2 - 30	3%	0.1%	–	< 10%	0.1%
30 - 120	3%	0.1%	–	< 10%	0.1%
120 - 160	2%	< 0.1%	–	< 5%	< 0.1%
160 - 200	2%	?	–	1%	?
200 - 300	1%	?	≲1%	< 1%	?

*Estimated in part from the book "The Solar Output and Its Variations" edited by O. R. White.

†Fraction of full scale (FS) for 0.1 - 2 nm because of large dynamic range; otherwise fraction of average level.

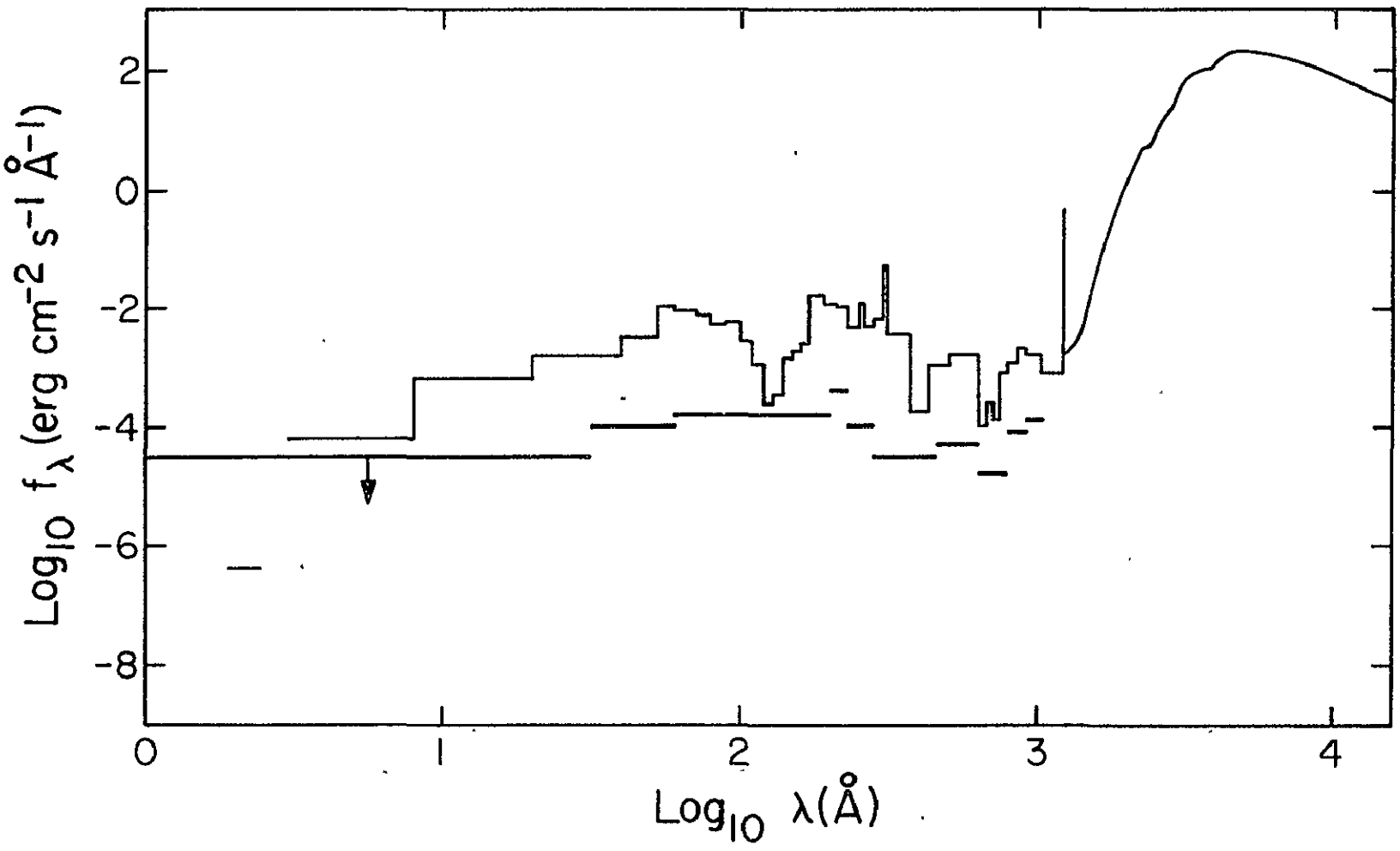

Figure 4-2. Flare Contribution to Solar Spectral Irradiance

A wavelength resolution of 2 nm would be sufficient to follow the rapid change in flux from 300 to 200 nm.

Solar atmosphere models vary in complexity and purpose. Here we can identify two categories. High-resolution models require the best state-of-the-art research instrumentation to provide very fine spectral, spatial, and temporal resolution. These are not applicable to our suggested support instrument. On the other hand, there is a need for models that treat special questions, such as the energy content of various temperature regimes of the solar atmosphere, and how the energy content varies with time and distribution over the disk. Some of these models need only moderate spectral resolution, accuracy, and sensitivity, and are applicable to a monitor instrument. Examples would be models of the solar activity cycle; a more specific case would be a model to relate the energy balance of flare or active region plasmas in each of the characteristic temperature ranges and to estimate the energy flow between temperature ranges. Solar atmosphere requirements in Table 4-2 are applicable to these models.

In conjunction with the above accuracy requirements, one must add that the instrument must be stable at its level of sensitivity, or else calibration must be built-in to account for drifts or shifts. In Space Shuttle operations there is an advantage that laboratory calibration is possible before and after each flight. If in-flight drift can be anticipated, there must be in-flight calibration.

4.5 *XUV MONITOR DESIGN CONCEPTS*

No single instrument is capable of covering the full range 0.1 to 400 nm under consideration in this report. Nor can the requirements of Table 4-2 be met entirely with simple instruments void of moving parts or sensitive optics. Our best present concepts of suitable instrumentation include three instruments in two categories.

Category A has two instruments that view the whole Sun. One of the two is derived from the NRL group. It covers the range 120 to 400 nm with the best available calibration accuracy and in-flight calibration, adequate time resolution and spectral resolution for both solar physics and aeronomy, and adequate sensitivity for all but flare energy content observations. The second instrument is derived from the Berkeley group. It covers the range 0 to 200 nm with calibration before and after flight, adequate time resolution for both disciplines, spectral resolution adequate for solar physics and useful for aeronomy, and sensitivity that is adequate to about 150 nm.

4.5.1 *The NRL Instrument*

A simplified block diagram of the instrument is shown in Figure 4-3.

4.5.1.1 *Experiment Description.* The Solar Ultraviolet Spectral Irradiance Monitor (SUSIM) consists of two identical double-dispersion scanning spectrometers, seven detectors (five photodiodes and two photon counters), and a UV calibration light source. The spectrometers

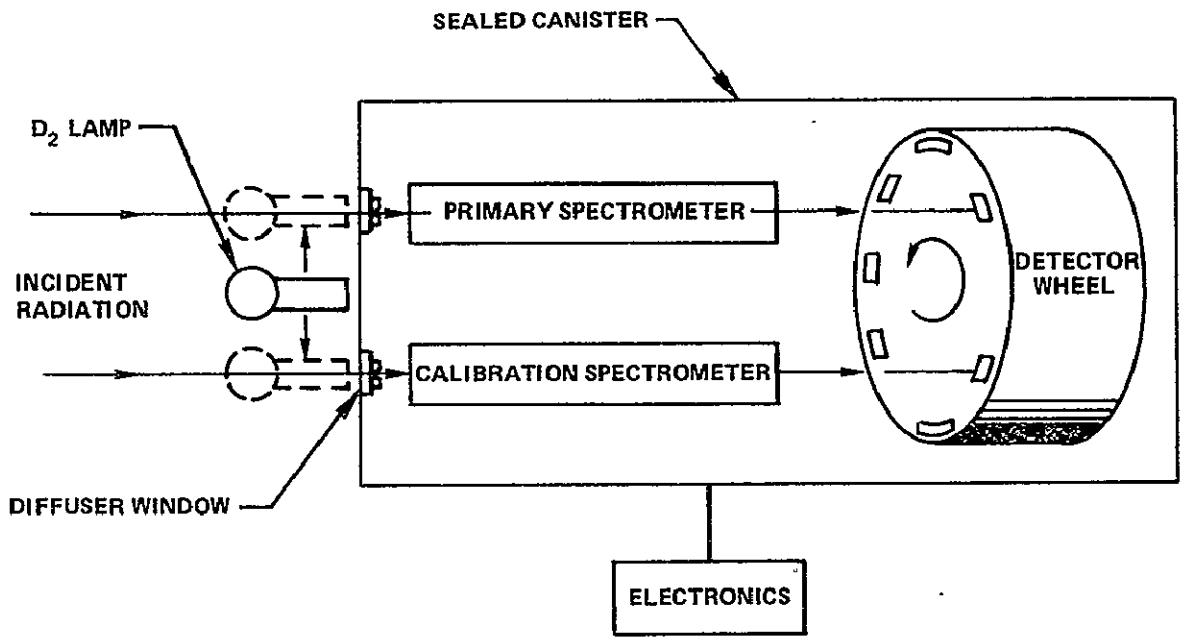

Figure 4-3. Block Diagram of NRL Instrument

and detectors are sealed in a canister filled with 0.1 atmosphere of argon to eliminate the effects of contamination due to high-vacuum outgassing.

One spectrometer is used almost continuously during the daylight portion of each solar pointed orbit to measure the short-time variations of the solar UV flux (flare related changes and the slowly varying component). The second spectrometer is used only once every day to track any change in sensitivity of the first spectrometer. Similarly, two of the five photodiodes are used only once every day.

A deuterium lamp, calibrated in spectral irradiance by the National Bureau of Standards (NBS), is used as the transfer standard source for daily in-flight calibration and stability tracking of both spectrometers and all seven detectors. A spectral resolution of 0.1 nm over the entire wavelength range is obtained with the two photon counters (operating in the stable pulse height discrimination mode) while 5-nm resolution is obtained with the five photodiodes (calibrated as transfer standard detectors by NBS). The instrument occupies a 15 by 20 by 30 cm volume with the 15 by 20 cm side facing the Sun. It weighs 9 kg (including the electronics) and has an average power requirement of 3.5 W and a data rate of 48 bps. (The external dimensions are somewhat flexible.)

4.1.5.2 *Modes of Operation and In-flight Calibration.* Three major operational modes are incorporated in the instrument.

a. Continuous Monitoring Mode

(1) Eight broad-band channels (5-nm resolution) will be monitored five times every solar pointed orbit (total observing time 15 min). The channels are chosen to monitor the Lyman-α line at 121.6 nm and seven segments of the solar continuum, ranging from 145 to 390 nm. This mode is designed to measure the slowly varying component and continuum changes with high accuracy.

(2) During the remainder of each orbit, eight narrow-band channels (0.1 nm resolution) will be monitored continuously. The channels include five important solar emission lines and three continuous segments. This mode can detect with high-time resolution (appr 2 min) flare related emission line changes and flux changes in emission lines caused by the slowly varying component and the 27-day cycle. The continuum scans are necessary for reference calibration.

b. Spectral Scan Mode. Once each day, the entire spectrum (120 to 400 nm) will be scanned with 0.1-nm resolution (total observing time - two orbits). This mode allows measurement of flux changes in all the remaining emission lines caused by the slowly varying component and the 27-day cycle.

c. In-flight Calibration Mode. Once every day a calibration and stability tracking measurement will be made. In the narrow-band mode, a spectral scan of both the solar spectrum and the deuterium lamp spectrum will be performed with each of the two spectrometers. In the broad-band mode, the eight channels mentioned above will be monitored with each spectrometer, using both the Sun and the deuterium lamp as the source.

This mode is designed to determine instrument changes of the prime spectrometer and detectors and to measure long-term solar flux changes. In order to detect long-term UV flux variations, it is necessary to determine changes in the instrument reflectivity and detector efficiency with high accuracy. It must be assumed that these changes are wavelength dependent. They can be determined using the Sun as a standard at 400 nm and the D_2 lamp's relative spectral output, which is known to be very stable.

4.5.2 *The Berkeley Instrument*

4.5.2.1 *General Concept.* The Broad-band Solar XUV Spectrometer consists of an array of nine chevron Channel Electron Multiplier Arrays (CEMA) followed by nine identical sets of electronics. In front of each CEMA, there is a transmission filter that defines the wavelength

response of that detector. A cylindrical collimator limits the field of view of each CEMA to ~ 10 deg. The total instrument package is 18 by 18 cm^2 in frontal area and 45 cm in depth. A side view of the package is shown schematically in Figure 4-4. The two filters in front of each CEMA are made of the same material but differ in thickness. While the thin filters are fixed, all the thick filters can be simultaneously moved out of the CEMA field of view with a dc brush motor.

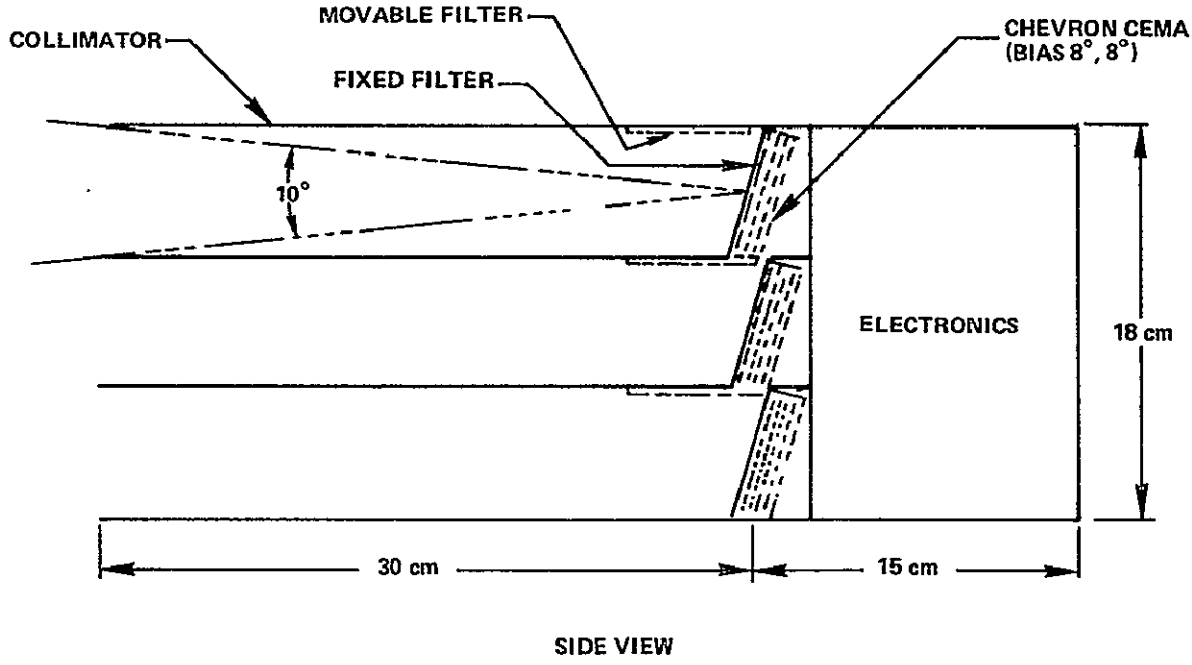

Figure 4-4. A Schematic Side View of the Broad-Band Solar XUV Spectrometer

4.5.2.2 *Detectors and Filters.* A chevron CEMA consists of two CEMA devices in tandem with a difference of approximately 16 deg in channel bias angle between the two devices. The chevron CEMA selected for this experiment is the model 3040, manufactured by Gallileo Electro Optics Corp., with a 12-micron pore size and 40-mm diameter. The channel bias angles (front/back) are about 8 deg/8 deg. Each CEMA is mounted with its normal at an angle of 17 deg with respect to the axis of the collimator (see Figure 4-4). Thus, the incident photons strike the CEMA channels at an angle of ~ 25 deg, near optimal for producing a peaked pulse-height distribution.

The nine detectors are operated at an electron gain of 10^6, which is about a factor of 10 lower than the gain at which these detectors are normally operated. This lower gain enables the CEMA to operate at a counting rate of ~ 1 to 5 X 10^6 pulses per sec.

The filters used with the nine CEMA are presented in Figure 4-5. The transmission of each filter τ_i (λ) and the efficiency ϵ_i (λ) of the corresponding CEMA for detecting a photon of wavelength λ determine the effective response r_i (λ) of the ninth detector

$$r_i(\lambda) = \tau_i(\lambda)\,\epsilon_i(\lambda) \quad \text{counts/photon}$$

where i = 1,2,. . .9 relate to the nine detectors. Figure 4-5 shows the response r_i (λ) computed from the available information on τ_i (λ) and ϵ_i (λ). The combined thickness of the two filters for each CEMA is selected to obtain a counting rate of 1×10^6 counts sec^{-1} at the output of each CEMA when the instrument is pointed towards the quiet Sun.

4.5.2.3 *Calibration.* An absolute calibration of the detectors will be carried out. A hollow cathode source of the type developed at Berkeley will be used to generate strong lines and continue in the 20 to 250 nm range of the spectrum. For the region below 20 nm down to the lower limit set by the monochromator (1 nm approximately), a Henke type ultrasoft X-ray source will be used that produces intense lines of the elements O, C, Si, Be, B, S, P, and aluminum. The radiation produced by these two sources is fed into a McPherson 2.2-m grazing incidence monochromator set at an incidence angle of 87 deg. In this way about 63 lines can be generated and isolated in the 2 to 200 nm region. All these lines have sufficient intensity to properly stimulate the flight instruments and the calibration standards.

4.5.3 *Beckers-Blake XUV Monitor Concept*

As outlined in the previous paragraphs, this third instrument constitutes category B. It is a single package but contains different detection schemes for the various wavelength ranges. It is essential for a support instrument that meets the maximum number of solar physics and aeronomy needs to have crude imaging capability (the category B distinction). To achieve this, the scheme outlined in Table 4-3 and Figure 4-6 was developed.

The basic concept shown in Figure 4-6 is that crude imaging was achieved with pin-holes. Since a resolution of several arc minutes is sufficient to locate the varying active region, pin-holes several mm in diameter can be used with detectors ~ 3 m away. Then diffraction is not a problem, even past 300 nm, and the only calibration required is on the detectors. There are no moving parts. Broad-band spectral resolution is obtained with filters. Time response and sensitivity can be very good over the entire range.

At the shortest wavelengths the pin-hole will not admit enough flux for imaging very fast. Therefore, one large area proportional counter (PC) is used with no pin-hole to get fast time response, and one position sensitive proportional counter (PSPC) is used to locate the event by integration over its duration. In the 1 to 200 nm range exactly the same scheme is used as the Berkeley group, except that a pin-hole is added to make the CEMA position sensitive by the design worked out by J. G. Timothy[12]. The photon flux is adequate over the full range. From 200 to 400 nm interference filters (20 nm FWHM) are used to define the spectrum incident upon a phosphor that converts the signal to photons > 400 nm.

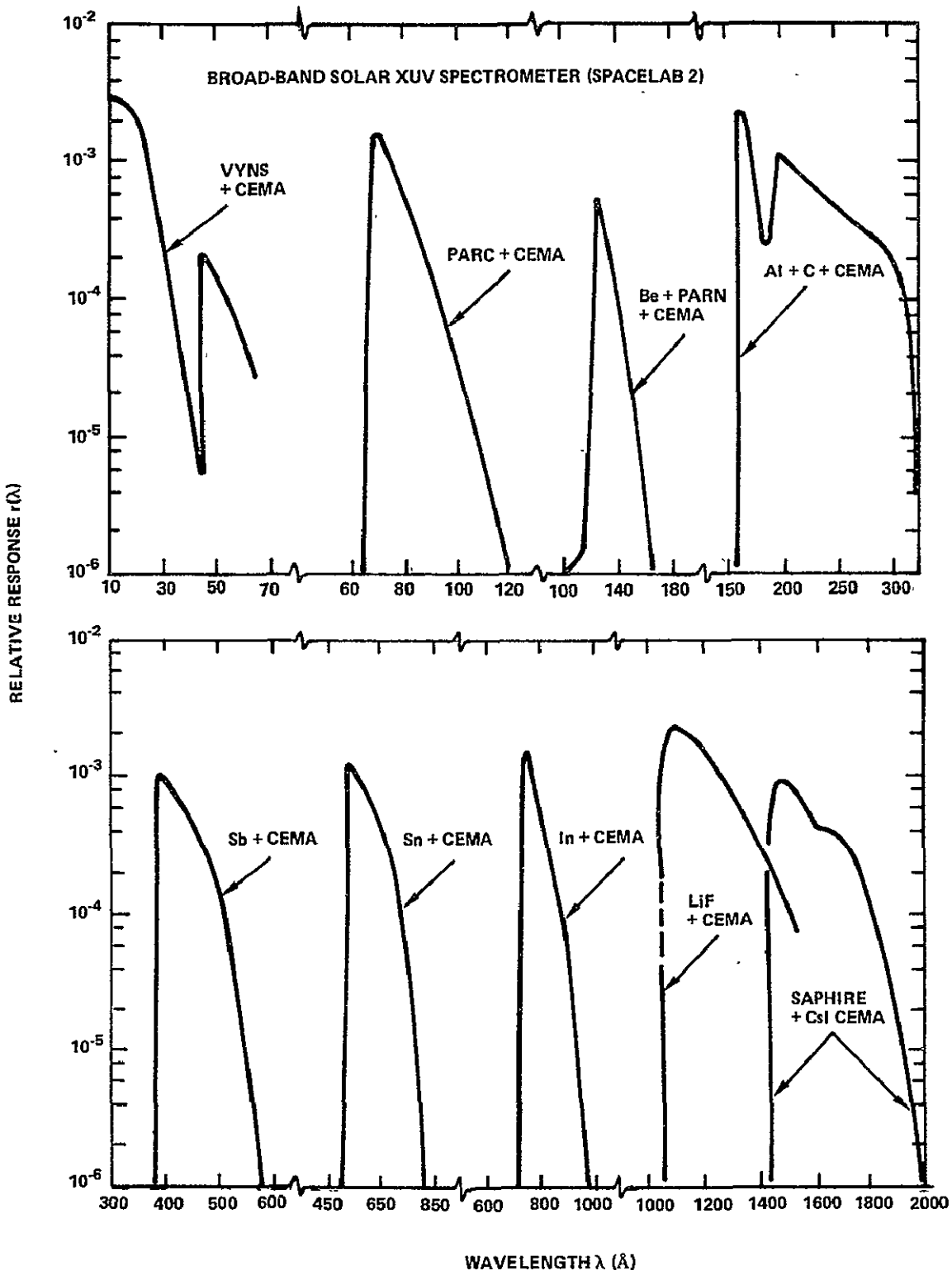

Figure 4-5. Response Characteristics of the Filter-CEMA Combinations (The short wavelength limit to the VYNS-CEMA response is determined by the rapidly decreasing photon number spectrum with decrease in wavelength.)

Table 4-3
Blake-Beckers XUV Monitor*

Wavelength Range (nm)	Detector	Filter	Wavelength Resolution (nm)	Time Resolution (sec)	Dynamic Range
0.1 - 0.3	PC	Be (window)	0.015 - 0.07	0.1	10^5
0.1 - 0.3	PSPC	Be (window)	0.02 - 0.10	10 - 100	10^4
0.3 - 1	PC	Be (window)	0.07 - 0.40	0.1	10^5
0.3 - 1	PSPC	Be (window)	0.10 - 0.50	10 - 100	10^4
0.8 - 1.5	CEMA	Aℓ	0.7	0.1	10^6†
1.8 - 2.5	CEMA	CF_2	0.7	0.1	10^6†
2.7 - 2.5	CEMA	Ti	0.8	0.1	10^6†
4.4 - 6.5	CEMA	C	2.0	0.1	10^6†
6.5 - 11	CEMA	PAR-C	4.5	0.1	10^6†
11 - 16	CEMA	Be + C	5.0	0.1	10^6†
17 - 40	CEMA	Aℓ + C	23	0.1	10^6†
40 - 50	CEMA	Sb	10	0.1	10^6†
50 - 80	CEMA	Sn	30	0.1	10^6†
75 - 90	CEMA	In	15	0.1	10^6†
110 - 140	CEMA	LiF	30	0.1	10^6†
145 - 185	CEMA	SAPHIRE	40	0.1	10^6†
140 - 160	Phosphor	Inter-	20	0.1	10^3
.	+	ference	20	0.1	10^3
.	Fiber	Filter			
.	optics				
.	+				
380 - 400	CCD				

*System uses pin-holes to cast crude images onto position-sensitive detectors through broad-band filters.

†Dynamic range given for detector; signal will be set near top of range to permit high sensitivity to detect changes in short time. Sensitivity in 10 sec is PC ~ 0.3 percent, CEMA ~ 0.1 percent, CCD ~ 0.1 percent.

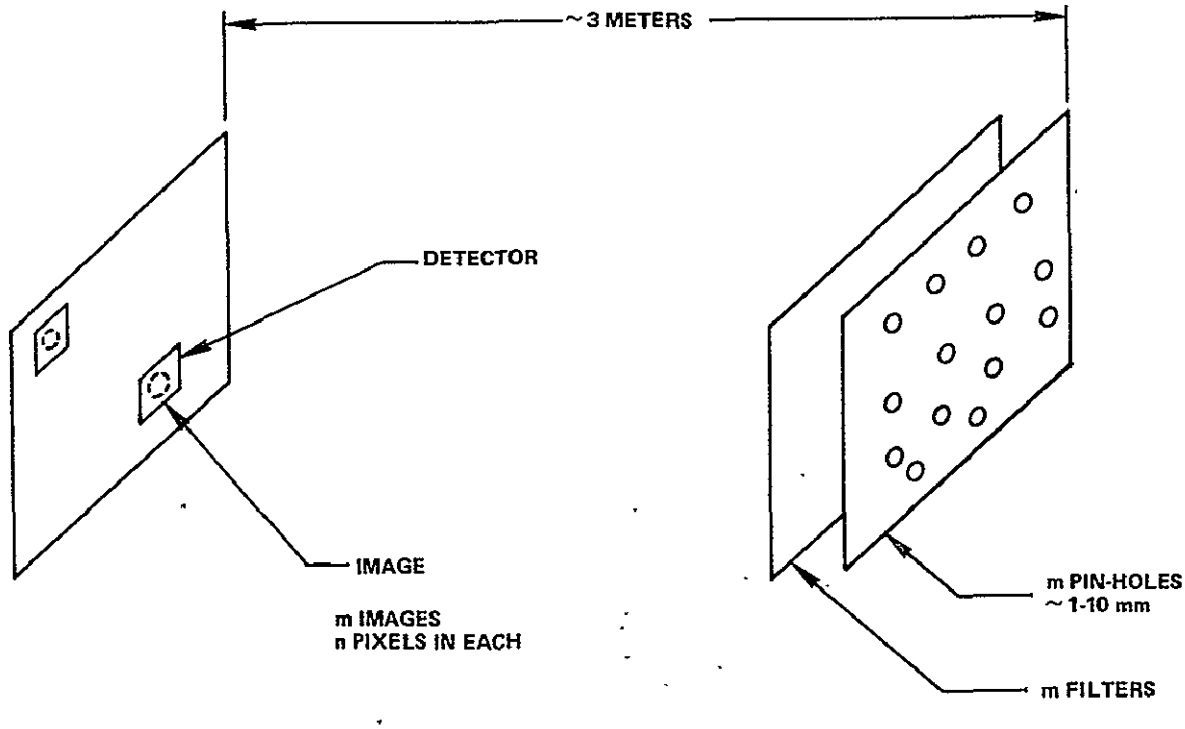

Figure 4-6. Blake-Beckers XUV Monitor Concept (The number of detectors is approximately equal to the number of passbands which should be about 25. The image size is roughly 30 mm with a resolution of 5' for 5 mm pin-holes.)

The converted photons are guided by a fiber optics bundle to a charge coupled device (CCD) that has the necessary position sensitivity.

This instrument meets all the requirements of a monitor for solar physics and aeronomy except the wavelength resolution needed for aeronomy for the non-flaring Sun. That requirement must be met by a separate instrument, which would logically be a special-purpose experiment carried out by a single PI team.

A more sophisticated version could have inflight calibration in the ranges < 1 nm and > 175 nm. For the intermediate range it is not clear that in-flight calibration is yet feasible except by carrying auxiliary windowless standard detectors.

REFERENCES

1. Smithson, R. C., "The Lockheed Diode-Array Magnetograph," Solar Phys., 40 (1), 1975, p. 241.
2. McIntosh, P. S., and R. F. Donnelly, Solar Phys., 23, 1972, p. 444.
3. Zirin, H., and K. Tanaka, Solar Phys., 32, 1973, p. 173.
4. Tucker, W. H., and M. Koren, Astrophys. J., Vol. 168, 1971, pp. 283-312.
5. Lin, R. P., and H. S. Hudson, Solar Phys., 17, 1971, p. 412; and preprint, "Non-thermal Processes in Large Solar Flares."
6. Kane, S. R., and R. F. Donnelly, Astrophys. J., Vol. 164, 1971, p. 151.
7. Mitchell, J. M., (to be published), 1977.
8. Eddy, J. A., "Physics of Solar Planetary Environments," D. J. Williams, ed., Vol. 2, 1976, pp. 958-972.
9. Hines, C. O., J. Atmos. Sci., (to be published).
10. Heath, D. F., "The Solar Output and Its Variations," O. R. White, ed., (to be published).
11. Donnelly, R. F., "Empirical Models of Solar Flare X-Ray and EUV Emission for Use in Studying Their E- and F- Region Effects," 1976 Preprint, J. Geophys. Res. (to be published).
12. Timothy, J. G., and R. L. Bybee, Appl. Optics, 14, 1975, p. 1632; and Rev. Sci. Instrum., 48, 1977, p. 292.